Test Methods for Characterization of Antibacterial Silver Organometallic Solutions on Textile Fabrics

by

Nicholas Kam

A thesis
presented to the University of Waterloo
in fulfillment of the
thesis requirement for the degree of
Master of Applied Science
in
Mechanical and Mechatronics Engineering

Waterloo, Ontario, Canada, 2019

Author Declaration

I hereby declare that I am the sole author of this thesis. This is a true copy of the thesis, including any required final revisions, as accepted by my examiners.

I understand that my thesis may be made electronically available to the public.

Abstract

Antimicrobial agents have been incorporated into textile fabrics to inhibit the growth of undesirable odor-producing bacteria. In recent years, a variety of consumer textiles have been commercially released that utilize active chemical agents to disrupt the working function of bacterial cells, e.g. *Stahylococcus aureus*, *Pseudomonas aeruginosa*, and *Escherichia coli*. As consumer products it is essential that testing be preformed to evaluate the overall efficacy of an antibacterial fabric surface.

This thesis was prepared in collaboration with Microbonds, Canada, and involves the investigation of their odor eliminating spray Go.Fresh. The primary antibacterial agent is silver complexed with organic molecules—organometallic silver—dissolved in an aqueous solution. Silver is an excellent antibacterial due to its low toxicity to humans. Application of the organometallic in aerosol form enables fine dispersal of the solution onto any textile material. Characterization and antibacterial efficacy tests were preformed on candidates for the commercial silver organometallic solution (SOS).

This thesis outlines scientific methods used to evaluate SOSs in application. Test methods are divided into three sections: characterization of the organometallic silver via standard analytical techniques; development of metrics for staining on fabric at various organometallic concentrations; and measurement of antibacterial efficacy on treated fabrics. Chemical analysis via energy dispersive X-ray (EDX) confirmed the presence of silver on treated fabrics. Concentration measurements on fabric via inductively coupled plasma optical emission spectrometry (ICP-OES) indicated a 49 % loss in silver from initially applied amounts. Staining on fabric was accurately measured using a Nix Pro colour sensor. Discolouration based on the CIELAB colour space was applied. Imperceptible changes in colour was generally observed in samples at silver concentrations below 100 ppm. Lastly, antibacterial properties of the SOSs were confirmed by minimum inhibitory concentration (MIC) tests that reported complete elimination of 99.9 % of bacteria. Accelerated methods proposed for antibacterial testing based on concentrations of adenosine triphosphate (ATP) correlated well with MIC results. Fabric samples treated with organometallic silver reported a 96.4 % reduction in ATP relative to an untreated control. Additional ATP tests showed comparable bactericidal power to that of standard copper surfaces.

Acknowledgements

I would like to thank Dr. Michael Mayer for his guidance throughout the project. I would also like to thank Dr. Bill Anderson for his support during biological studies and access to lab equipment. I would like to acknowledge the assistance from the National Science and Engineering Research Council (NSERC) through their financial support. This work was prepared in collaboration with Microbonds Inc., the manufacturers of Go.Fresh, who provided material support and counsel. Lastly, I would like to thank the following colleagues: Sanjay Krishna for his guidance in antibacterial testing; Mostafa AbdelAziz and Sudharsan Venkatesan for their invaluable advice; Jane Siu for her assistance in preparing fabric samples; and Ian Lung for his help with sample imaging in the staining study.

Table of Contents

List of Figures

List of Tables

Chapter 1 | Introduction

1.1 Motivation and Objectives

This thesis presents methods to evaluate the efficacy of silver-based organometallic solutions (SOSs) manufactured by Microbonds, Toronto, Canada. Go.Fresh is a commercial SOS that applies trace amounts of silver onto textiles to prevent the formation of odor. The organometallic compound is designed to chemically bond to fibers—particularly organic based—to attain strong adhesion and provide continuous elimination of bacteria. Dispensing of the SOS via aerosol spray enables easy application onto garments, see Figure 1.

Figure 1 Antibacterial organometallic silver spray Go.Fresh.

Silver has historically been used as a disinfectant due to its low toxicity to human cells [1]. Complexion of metals with organic molecules act as method of stabilization for silver ions and enables the antibacterial agent to be dissolved in aqueous solution. Methods detailed in this thesis are intended to evaluate the application of SOSs on a scientific basis. Initial investigations were performed on 19 overall candidate solutions, composed of different solvents at varying silver concentrations. Documented studies are primarily focused on the commercial water-based 100 ppm Ag formulation, though additional SOSs are discussed on a comparative basis. Characterization of any commercial antibacterial product is critical to ensuring its safe and suitable use by consumers. Results established here can be used in support of regulations required for access to Canadian markets.

Objectives in evaluation of the SOSs are divided into three sections:

- Analytical methods to characterize the silver organometallic in various forms and applications (i.e. solid, liquid and on fabric), presented in Chapter 2.

- Development of a quantitative method for measuring silver stains on fabrics due to the accumulation of organometallic deposits, presented in Chapter 3.

- Antibacterial efficacy testing on treated fabrics based on standard and proposed methods, presented in Chapter 4.

1.2 Biology Background for Antimicrobial Activity

Antibacterial agents are defined as chemical compounds that specifically target bacteria by destroying or inhibiting growth of the cell [2]. Their integration with textiles has enabled functionalization in various commercial products including sportswear, healthcare, food packaging, air filters and water purification [3]. Antibacterial treatment of textiles function to either protect the fabric from the effects of bacterial growth (anti-odor) or to protect users from harmful microorganisms (infection prevention). Antimicrobials most commonly used in commercial textiles include polysaccharides like chitosan, disinfectants such as Triclosan ($C_{12}H_7Cl_3O_2$), quaternary ammonium compounds (QACs) and metal ions, particularly silver-based coatings [4]. A comparative study of these antibacterial compounds performed by Windler et al. concluded that silver textile coatings could achieve high functionality at very low rates of application, offering obvious benefit to future antimicrobial textiles [5]. The purpose of this section is to provide a general biological background in support of experimental methods.

1.2.1 Bacteria Biology

Bacteria are prokaryotic cells, unicellular organisms that contain all functional intracellular sub-units in a single-phase cytoplasm enclosed by a cellular membrane. Prokaryotes lack the large compartmentalized organelles found in eukaryotes, with most metabolic reactions occurring within the cytoplasm. Bacteria can behave as a population by a process known as quorum sensing, extracellular signaling via secreted chemical factors to communicate and sense population density. Gram-negative bacteria *Pseudomonas aeruginosa* has been observed to use quorum sensing to form biofilms that enable adherence to body surfaces and improves its resistance to antibiotics [6].

Bacteria is classified by their metabolic mechanisms as either heterotroph or autotroph. Heterotrophs consume and breakdown external organic compounds as energy sources, and include species that undergo fermentation or respiration (e.g. odor forming bacteria). Bacteria capable of producing their own energy, fueled by light or chemical reactions, are known as autotrophs. Heterotrophic bacteria cells utilize metabolic reactions to convert nutrient resources into cytoplasm and increase in biomass. Growth is regulated by biological pathways based on nutrient availability and is linked by genetic factors. At a critical size chromosome replication is initiated, triggering the cell to undergo asexual reproduction by binary fission. Bacteria reproduction occurs at exponential rates dependent on the strain of bacteria. In favorable conditions *Escherichia coli* has been observed to undergo chromosome replication in 40 mins and cell division in as little as 20 minutes [7].

1.2.2 Odor Forming Bacteria

The primary function of the SOSs is the elimination of odor forming bacteria on the surface of the skin. Human skin naturally supports a microflora of non-pathogenic organisms that serve one of two primary functions: acting in commensal symbiosis with the host or as a protective force against external pathogens. In the case of body odor, one evolutionary theory for its necessity is in its use as olfactory cues for kinship detection and mate selection [8]. Clothing garments maintain intimate contact with surface skin organisms, creating a warm-moist environment suitable for bacterial growth. Studies on axillary (armpit) odors identified bacteria species, *Corynebacterium* and *Staphylococci*, as primary contributors to malodor using 16S ribosomal RNA gene sequencing technique [9]. In the study, *Corynebacterium* was observed to be more present in adult males and *Staphylococci* in females resulting in distinctive gender-specific body odors. In other studies, bacterial species of the *Bacillus* (rod-shaped) genus have been linked to strong foot odors, and their use as test organisms in the control of odor on textiles have been recommended—e.g. *Escherichia coli* [10].

Body odor in adult humans is mediated primarily by the bacterial decomposition of sweat compounds naturally secreted from eccrine, apocrine, and sebaceous glands. Human perspiration consists mainly of water, with 0.2 % – 1 % solutes containing bacterial nutrients such as fatty acids, amino acids, glycerol, and lactic acids. Metabolic degradation of these nutrients results in a byproduct of odorous molecules (e.g. acetic acid, volatile fatty acids, sulfanyls, and thioalcohols) commonly associated with body odor [11].

1.2.3 Silver-Based Antibacterial Agents

Silver is an established antibacterial used for centuries in wound treatment due to its low toxicity to human cells relative to bacterial cells. The bactericidal effect of silver is attributed to the high reactivity of its ionized form silver(I). Ionized silver has been observed to bind and complex to the surface membrane of bacteria, killing cells by lysis. Silver has also been observed to bind to nucleic acids, RNA and DNA, to a lesser extent. Optical imagining performed on silver treated *Pseudomonas aeruginosa* found that a majority of Ag ions would localize at the cellular membrane, with less than 3 % in the RNA fraction and 12 % in the DNA fraction [12]. The targeting of multiple abiotic pathways by silver-based antimicrobials limits the ability for bacteria to develop resistance, securing their long term survivability in the market.

Escherichia coli is known to be semi-resistant to silver, with complete inhibition of bacteria reported at minimum concentrations of silver nitrate between 0.25 – 5 mM [1]. Use of these bacteria in antibacterial experiments thus represent an extreme case, with application to less resistant odor-forming bacteria expected to have increased effectiveness.

Various methods have been developed to incorporate silver to textiles fabrics. Silver particles suspended in a polymeric hydrogel have been applied to the medical field as wound dressings for the treatment of skin conditions [13]. Polymer matrices are typically used for silver-based coatings to stabilize the high reactivity of silver cations. In another example, researchers at North Carolina State University proposed the use of plasma technology and electrospinning to synthesize durable antibacterial Ag/polyacrylonitrile (Ag/PAN) hybrid nano fibers. Nanoparticulate silver embedded in a smooth continuous nanofiber matrix was shown to maintain extended silver ion release with robust

antibacterial activity [14]. Silver complexed with organic molecules act as another method of stabilization and benefits from direct adhesion to organic fibers without the need of an intermediary layer. This evasive method of bonding makes their application in anti-odor fabric an attractive option. N-heterocyclic carbenes (NHCs) are one class of organic compounds commonly used as carrier ligands for Ag ions. Commercially sold under the name Silvamist, Ag-NHC organometallics exhibit excellent antibacterial activity, although higher cytotoxic effects have been reported against mammalian cells [15].

Go.Fresh falls under this categorization of silver-based organometallics, and is designed for safe use in anti-odor on consumer garments. Previous studies by Campbell et al. [16] at the University of Waterloo investigated a preliminary version of the organometallic formula containing extremely high levels of silver designed for fabric metallization. The reduction of silver to ppm levels has enabled the organometallic silver solution to be applied to the control of odor on garments. The silver-based organometallic is composed primarily of water (99 %) with the addition of proprietary resins and surfactants in combination with aromatic and glycolic solvents. Complete chemical composition of SOSs manufactured by Microbonds are not disclosed due to the commercial nature of the product.

Chapter 2 | Silver-Based Organometallic Characterization

The objective of chemical analysis performed on the primary SOS (water-based 100 ppm Ag) is to monitor silver levels throughout application to characterize the stability and lifetime of the antibacterial product. Confirmation of silver presence on fabric and measurement of silver concentrations in solution are critical to establishing product quality. Section **Error! Reference source not found.** analyzes the m orphology and composition of the pure silver organometallic powder using SEM/EDX and XRD techniques. Section 2.3 presents a microscopic view of staining on fabric via SEM imaging with EDX analysis. Section 2.4 details analysis of treated fabrics using Raman spectroscopy. Finally, Section 2.5 describes methods to measure the concentration of silver in both liquid form and on treated fabrics using ICP-OES. Equipment used for chemical analysis was provided by WATLab, Department of Chemistry and the Chemical Engineering Department at the University of Waterloo.

In summary, results of analytical testing show that SEM/EDX are best for determining the presence of silver on fabrics. EDX spectrums exhibited low signal-to-noise due to overriding carbon signals generated from fibers and was exacerbated at larger scan areas. This technique is therefore not recommended for measurement of relative concentrations on treated fabric. Precise measurement of silver concentration is best determined by ICP-OES analysis. Results from XRD and Raman spectroscopy analysis resulted in inconclusive evidence for silver, primarily due to the lack of reference patterns and the overpowering effect of fabric.

2.1 Characterization Methods for Silver Organometallics

This chapter presents characterization of the principle SOS using three analytical techniques established from literature. The first technique discussed is energy dispersive X-Ray (EDX). EDX is a common technique used for elemental analysis that relies on the characteristic excitation of electrons. This technique has been applied by A. Abou-okeli (2012) to identify the composition of silver nanoparticles bonded to pre-treated chitosan coated fibers [17]. X-ray diffraction (XRD) technique was also used in the study to analyze the crystallinity of particles and to verify EDX results. In similar studies performed on cotton fabrics modified with silver nanowires, surface-enhanced Raman spectroscopy (SERS) was used to identify the presence of silver on fabric by Puchowicz et al. [18]. The addition of silver nanoparticles was discovered to enhance Raman signals, with characteristic silver peaks measured at 237 cm^{-1}. Lastly, inductively coupled plasma optical emission spectrometry (ICP-OES) is a standard method for measuring elemental concentrations, popular in the analysis of soil samples and dissolved minerals in water. This technique has been recently used to measure silver content on commercially coated cotton fabrics and silver release over repeated wash cycles [19], [20].

2.2 SEM/EDX Analysis of Silver Organometallic Powder

Morphology of the pure silver organometallic complex was characterized using a FEI Quanta Feg 250 environmental scanning electron microscope (ESEM) with EDX analysis (WATLab, Department of Chemistry). To accomplish this, 200 µL of the primary SOS (water-based 100 ppm Ag) was pipetted directly onto conductive carbon tape and placed into the ESEM. Low vacuum pressures evaporate the water solvent leaving behind the organometallic silver in solid form, shown in Figure 2. Two distinctive structures were observed: a large coral-type solid constituting a majority of the powder, and a spherical flower-shaped structure. Both structures appear to form from the clustering of individual nanosized pellets. The coral shaped silver was observed to range in sizes between 10 - 100 µm across and the flower shaped structure between the ranges of 5 – 10 µm.

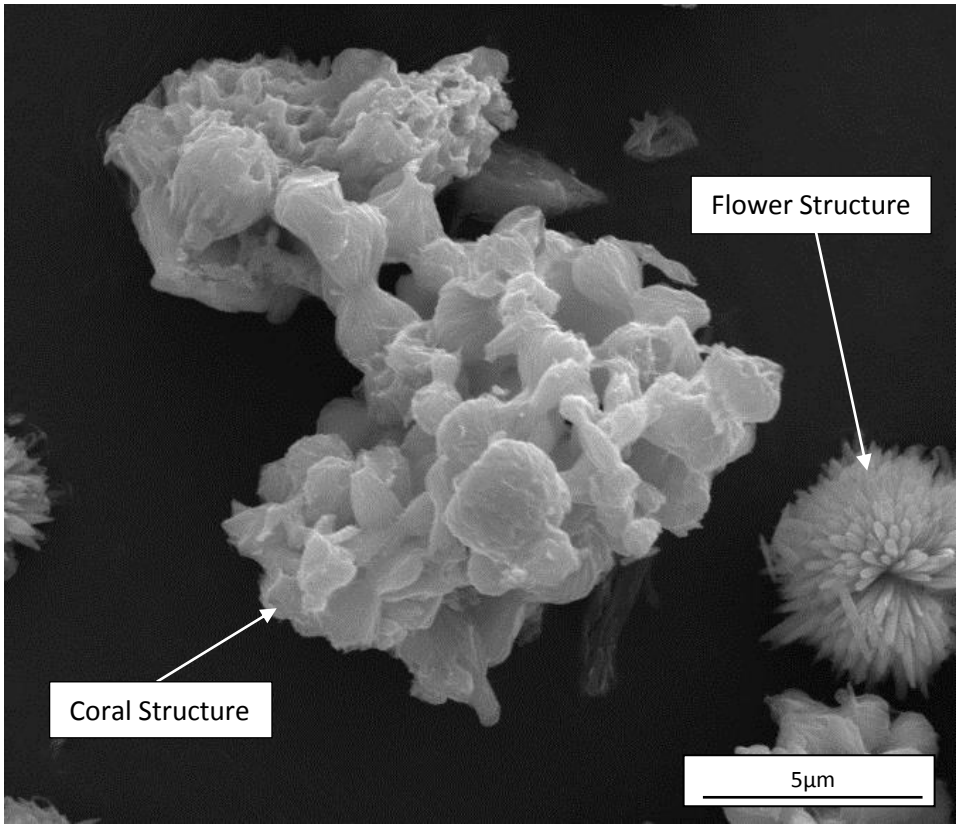

Figure 2 SEM image of silver organometallic particles (WATLab, Department of Chemistry).

The observed silver structures have been previously identified in literature. The coral-type structure is similar in morphology to silver organometallic complexes synthesized by Won et al. [21]. In the study, the formation of macroporous silver was accomplished by placing Ag nanoparticles in a solution of formic acid. Electron exchange during the reduction of formic acid leaves ionized silver in an unstable state. Silver ions begin bonding to neighboring ions to form the final coral-type structure, a slow reaction reported to yield clusters ranging from 1 -120 µm in length. The flower-type structure has also been observed before by El-Nagar et al. [22], where synthesis was achieved by a wet-chemical method involving the reduction of silver nitrate with ascorbic acid in the presence of succinic and malonic acid. Formation and stability of these flower-like structures were heavily dependent on temperature, mixing ratios of reactants and pH of the solution—with sizes controlled in the micron range. Formation of silver structures in the principle SOS could similarly be controlled by environmental conditions and the availability of neighboring silver ions during drying. Observed morphologies for the primary silver organometallic is thus consistent with silver structures reported in literature.

Elemental composition of the SOS in powder form was analyzed in situ by EDX analysis. Spectrum results indicate particles are composed primarily of silver by weight, with carbon and oxygen elements of the organic molecule forming the remaining composition—see Table 1. Elements present in the spectrum are consistent with the presumed silver organometallic complex, with possible overestimation in carbon content due to the substrate used (i.e. carbon tape). EDX results of powdered particles are used for comparison of elemental analysis on treated fabrics.

Table 1 EDX analysis of silver-based organometallic powder

Element	Weight %	Atomic %
C	18.76	50.10
O	15.40	30.87
Ag	61.78	18.37

XRD analysis was also performed on the silver organometallic powder using a Bruker D8-Focus XRD (Department of Chemical Engineering). The liquid organometallic was dried, and the powder collected for analysis—XRD pattern given in Figure 3. Lack of distinct diffraction peaks indicate a primarily amorphous structure consistent with the reduction in crystallinity associated with organic molecules. A significant diffraction peak occurs at 2θ = 34°. This singular peak could be evidence of a silver complex, as metallic silver is known to exhibit a diffraction peak at 38° corresponding to the (1 1 1) Miller Indices [23]. In addition, increased mixing ratios of organic compounds to metal have been demonstrated to shift diffraction peaks in organometallics [24], possibly explaining the 4° shift observed in the SOS XRD pattern.

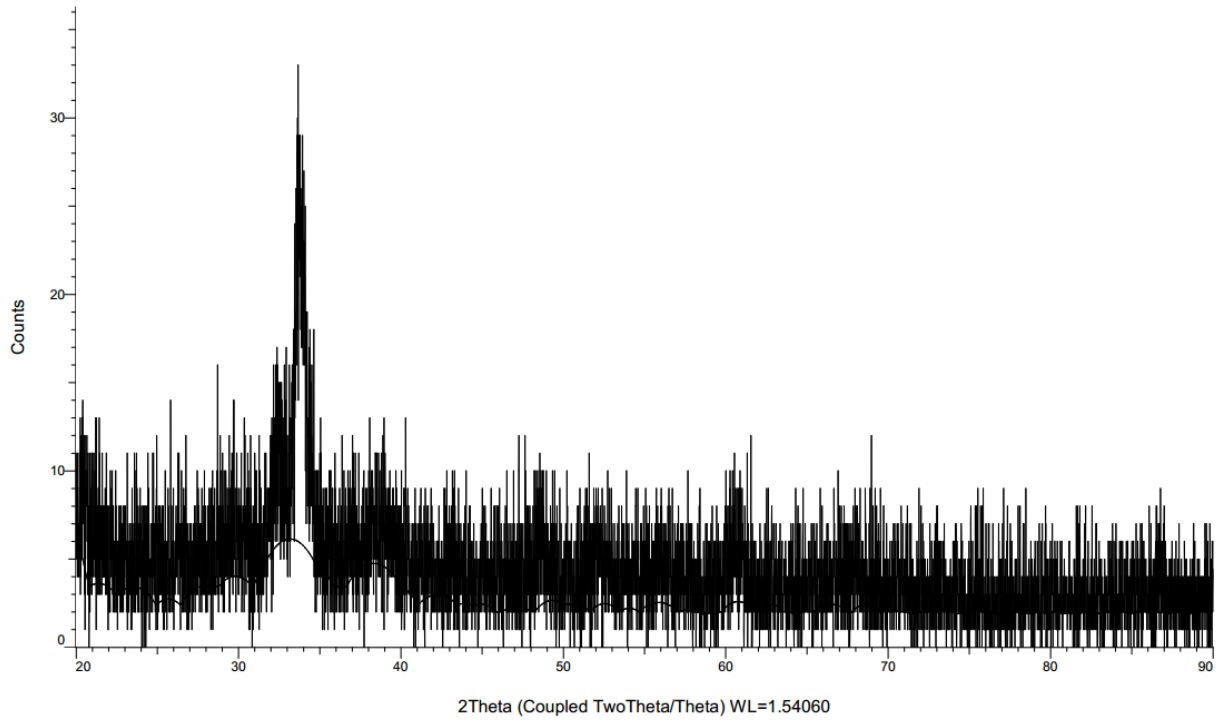

Figure 3 XRD diffraction pattern for silver organometallic in solid powder form (Department of Chemical Engineering).

2.3 SEM/EDX Analysis of Silver Treated Fabrics

To provide a physical perspective of staining due to application of the primary SOS, images of treated fabrics were taken using an Olympus STM6 microscope (Department of Mechanical Engineering) and a UltraPlus FESEM with EDX (WATLab, Department of Chemistry)—see Figure 4. Accumulation of silver is observed by yellow fibers where organometallic liquid was absorbed and active adhesion of the metal occurred. SEM images in Figure 4 c) and d) identify individual organometallic particles adhered to cotton fibers. At this magnification, silver particles are shown to be more discrete and sparsely deposited along fibers. The effective addition of these individual particles results in the overall discolouration observed macroscopically as a stain.

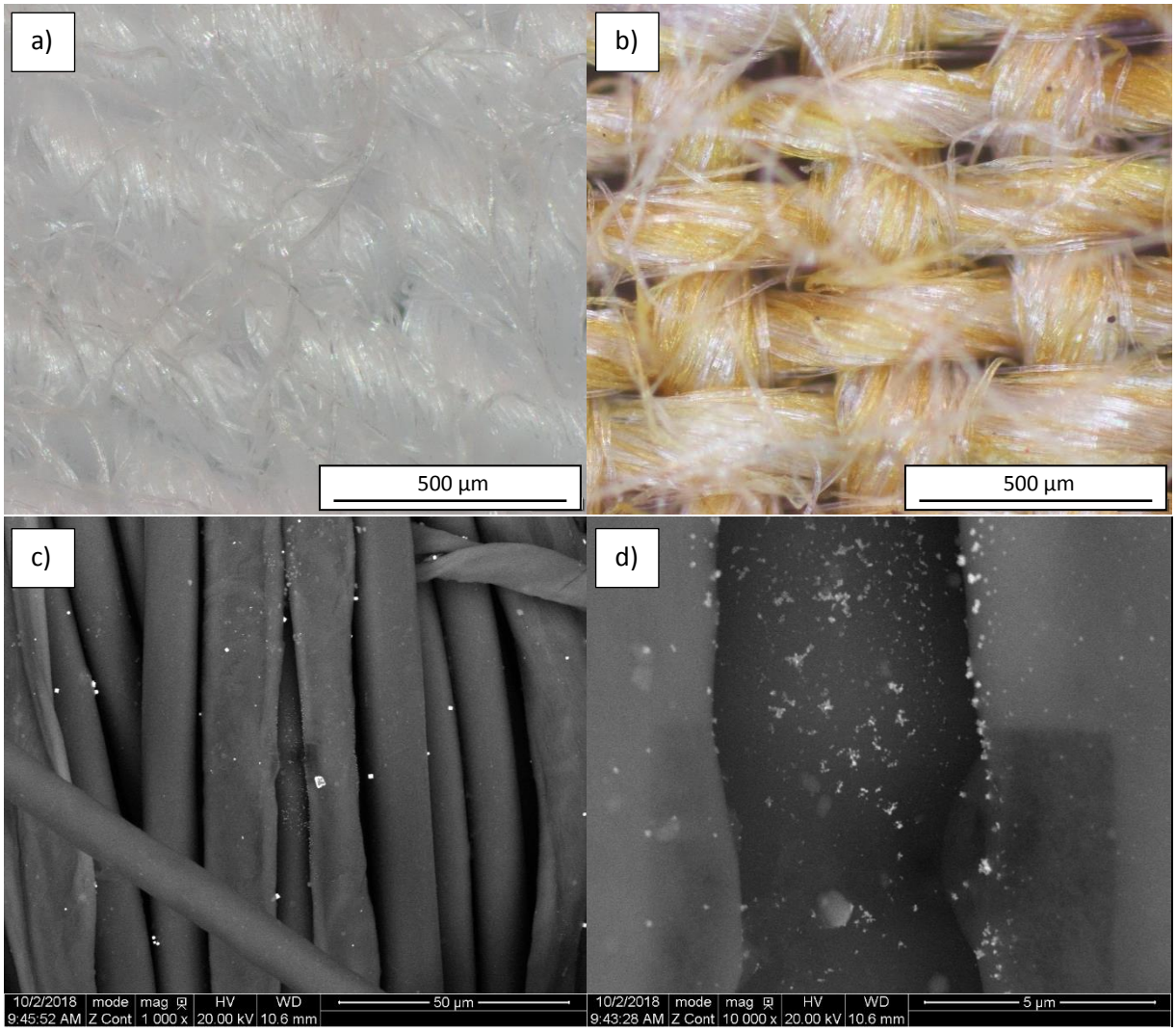

Figure 4 Optical images of a) untreated and b) treated cotton fabrics (Department of Mechanical Engineering); SEM images of treated fabrics at c) 1000x and d) 10000x magnification (WATLab, Department of Chemistry).

EDX analysis was also performed on SOS treated fabrics in order to estimate relative concentrations of applied silver. Regions were scanned in a 1 mm square area for a cotton fabric treated with 200 µL of SOS and compared relative to an untreated control, see Figure 5 and Figure *6* respectively.

Element	Weight %	Atomic %
C	46.38	54.40
O	51.61	45.45

Figure 5 EDX analysis of untreated cotton in a 1 mm^2 scan area (WATLab, Department of Chemistry).

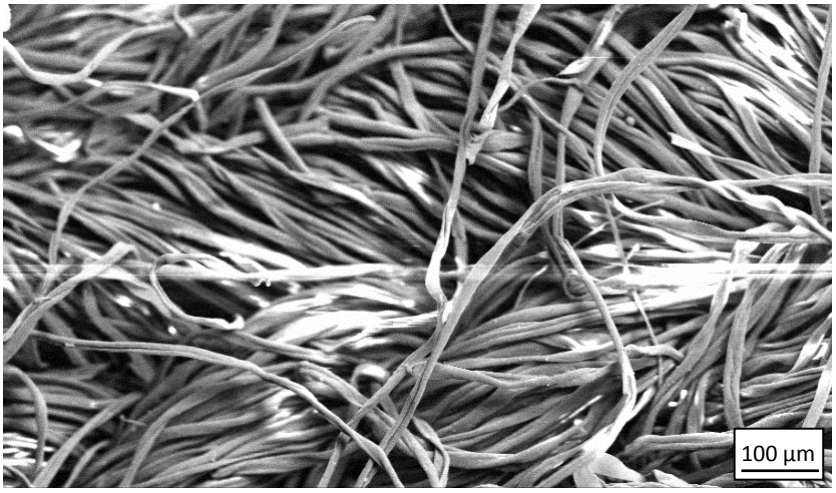

Element	Weight %	Atomic %
C	46.16	54.37
O	51.40	45.45

Figure 6 EDX analysis of cotton fabric treated with the water-based 100 ppm SOS in a 1 mm^2 scan area (WATLab, Department of Chemistry).

Chemical compositions of both spectrums indicate no presence of silver, with intensity peaks identifying primarily carbon and oxygen atoms present in the cellulose fibers. Accuracy of EDX analysis is strongly dependent on uniformity of the surface and not ideal to porous fibers. Lack of any observed silver peaks suggests that the concentration of silver may be below the machine detection limit of 1 wt. %. In addition, the general abundance of carbon present makes analysis difficult due to overriding signals. Analysis of the organometallic silver on fabric via EDX is therefore rendered inaccurate at the current magnification.

EDX analysis performed at higher magnification was able to measure relative concentrations of silver when focused on particle deposits attached to fibers—shown in Figure 7. Particle sizes were measured to be on average 10 µm across. EDX analysis of the particle complex detected low amounts of silver along with trace amounts of chlorine. Silver concentrations were significantly reduced from the pure solid analysis (62 % down to 9 %), an effect of overpowering signals from the carbon and oxygen elements in cotton. Adherence of silver organometallic particles to the cotton surface was thus confirmed in minimal amounts, below detectable limits in larger scans. Detection of chlorine atoms in the spectrum could be a result of residuals from dissolved minerals in the solvent water, forming silver chloride on fabric.

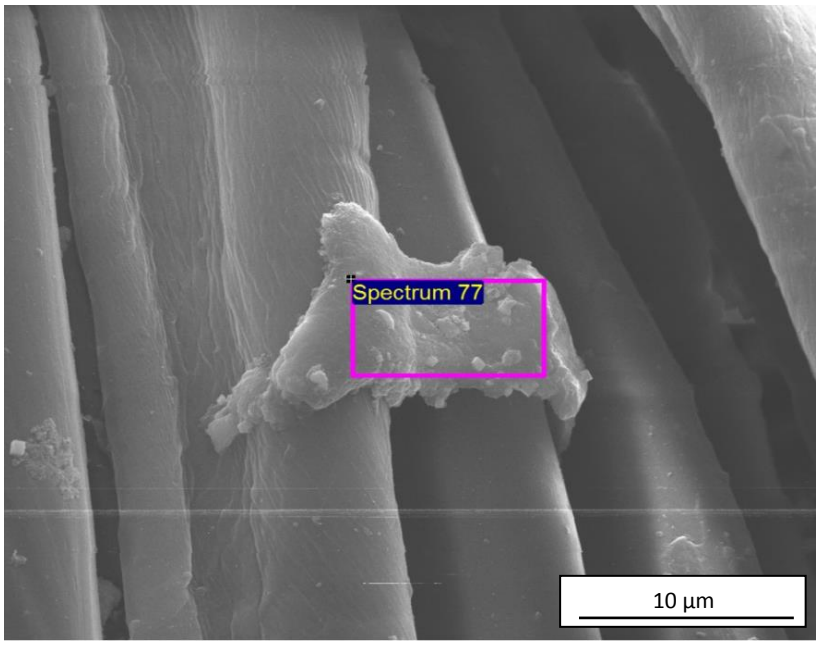

Element	Weight %	Atomic %
C	49.60	63.19
O	35.38	33.84
Ag	9.23	1.31
Cl	3.15	1.36

Figure 7 EDX analysis at high magnification focused on organometallic particles adhered to fibers (WATLab, Department of Chemistry).

2.4 Raman Spectroscopy Analysis of Silver Treated Fabrics

Previous studies have been performed by Kavler and Demšar (2011) [25] on the application of micro-Raman spectroscopy for the examination of fabrics. Characteristic peaks of cotton were compiled from a spectral database of modern cellulose fibers and is listed in Table 2. The data is used for the analysis of Raman shifts resulting from the principle SOS. Presence of silver on treated cotton fabric was analyzed via Raman Spectroscopy using a Bruker Senterra-2 Raman (WATLab, Department of Chemistry). Detection of cotton peaks is possible near infrared range; an excitation source of λ = 720 nm, 50 mW was applied.

Table 2 Characteristic Raman peaks for cotton fabrics.

Raman Shift [cm^{-1}]	Bond Description
330, 383	CCC, CCO ring deformation
437, 461	CCC ring deformation
523	glycosidic linkage COC
902, 1001	CH skeletal rotating
1101	COC in glycosidic linkages - symmetrical stretching
1122	COC in glycosidic linkages - asymmmetrical stretching
1344	CH2 vibrations
1385	CH2 vibrations
1484	CH2 vibrations
2900	CH stretching

Raman spectrums were obtained for a SOS treated fabric (200 µL) against an untreated control, given in Figure 8. For the control cotton spectrum, characteristic peaks for glycosidic linkages were detected at 520 cm^{-1}, 1097 cm^{-1} and 1123 cm^{-1}. Strong peaks of stretching C-H bands at 2907 cm^{-1} and weak bending CCC ring at 380 cm^{-1}, 435 cm^{-1} and 460 cm^{-1} were also observed. The Raman spectrum for the silver treated sample showed little difference to the control, with exception between the range of 100 cm^{-1} and 300 cm^{-1}. In this region, silver sample peaks appear more corrected compared to the upward shift in the control sample. Similar studies performed by Puchowicz et al. using surface-enhanced Raman spectroscopy detected characteristic silver peaks in a similar range (237 cm^{-1}) and found that the presence of silver nanoparticles enhanced Raman signals [18]. This suggests that the elimination of shifted peaks observed in the treated sample is evidence of silver organometallic presence on cotton. The lack of distinctive silver peaks is likely a result of low signal-to-noise ratio due to the porous nature of fabrics and the generally low silver content as determined by EDX analysis. Raman spectroscopy is therefore not recommended for measurement of silver concentrations.

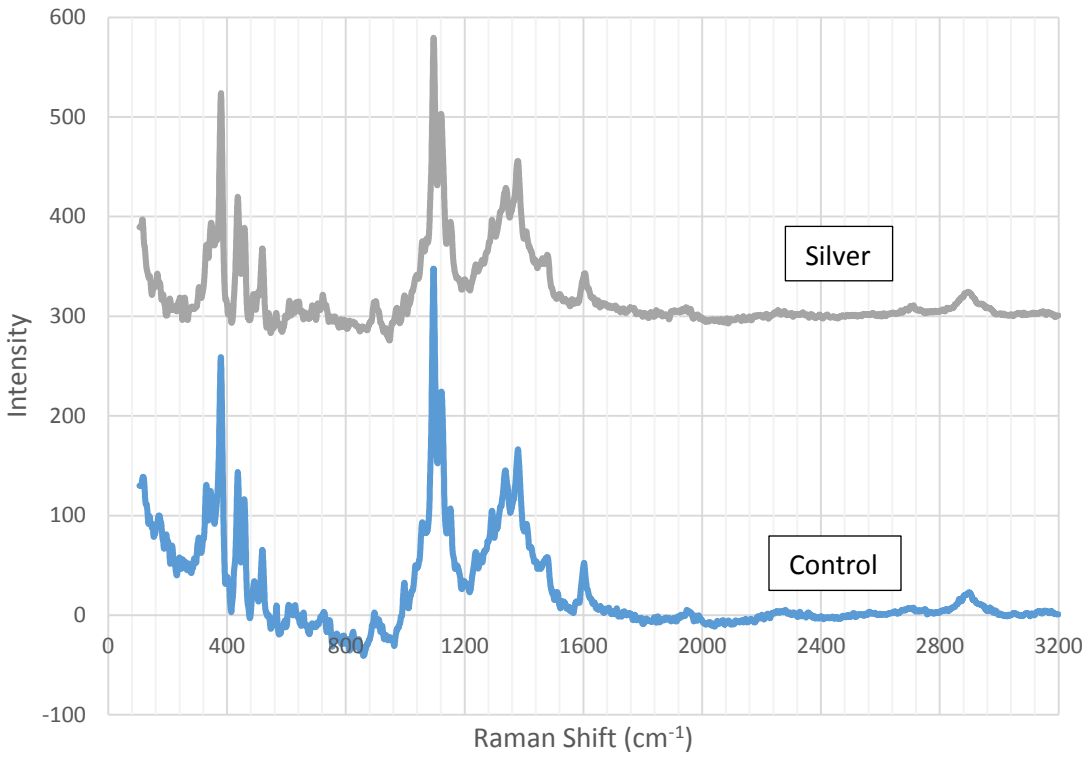

Figure 8 Raman spectrums for cotton fabric treated with SOS (200 µL) and an untreated control.

2.5 ICP-OES Analysis of Silver Treated Fabrics

ICP spectrometry is a standard method for measuring elemental concentrations. Measurement of silver content in SOSs was performed using a ProdigyPlus ICP-OES (Department of Chemical Engineering). Concentrations of silver was measured in both liquid solution (storage) and on fabrics (applied). Monitoring silver levels in solution provides information on the stability of the silver organometallic over time and can be used as a benchmark for product lifetime. Analysis on fabric provides information on the applied silver content during usage and can support guidelines for procedural application of the antibacterial spray.

2.5.1 ICP-OES Analysis of Silver Organometallic in Solution

ICP analysis was performed in triplicate on SOS at various Ag concentrations, results given in Table 3. Calibration standards at 5, 10, 25, 50 and 100 ppm Ag were prepared using silver nitrate in 5 % nitric acid. Dilutions were performed for samples with expected concentrations above 100 ppm Ag.

Table 3 Silver concentration of organometallic liquid solution at various concentrations via ICP-OES (Department of Chemical Engineering)

Expected Ag Concentration (ppm)	10	25	100	2000
Measured Ag Concentration (ppm)	7.0	22.4	86.7	1729.6
Standard Deviation	0.2	0.9	2.1	121.5
Percent Drop	30 %	10 %	13 %	14 %
pH	>9	>9	>9	>9

In general, concentrations of silver were close to the expected amount with an average drop of 12 % (excluding the 10 ppm Ag sample). The pH levels of all solutions were measured to be above 9 using standard litmus paper. Reductions in silver concentration was predicted to be caused by the precipitation of silver at higher pH levels. Silver(I) ions are known to drop out of alkaline solutions at pH levels above 9 to produce solids like silver hydroxide [26]. Precipitates formed in solution are highly dependent on the reactant chemicals; due to the proprietary nature of Go.Fresh exact mechanisms for silver drop out could not be determined.

Precipitation of silver was investigated over an extended period of 6 months on samples stored at room-temperature in transparent glass jars, shown in Figure 9. SOSs were exposed to artificial room light for an estimated 20 hours a week. Significant dropout over time can be observed by the physical change in colour of the solutions—initially translucent to an opaque brown—and the collection of precipitate settled at the bottom.

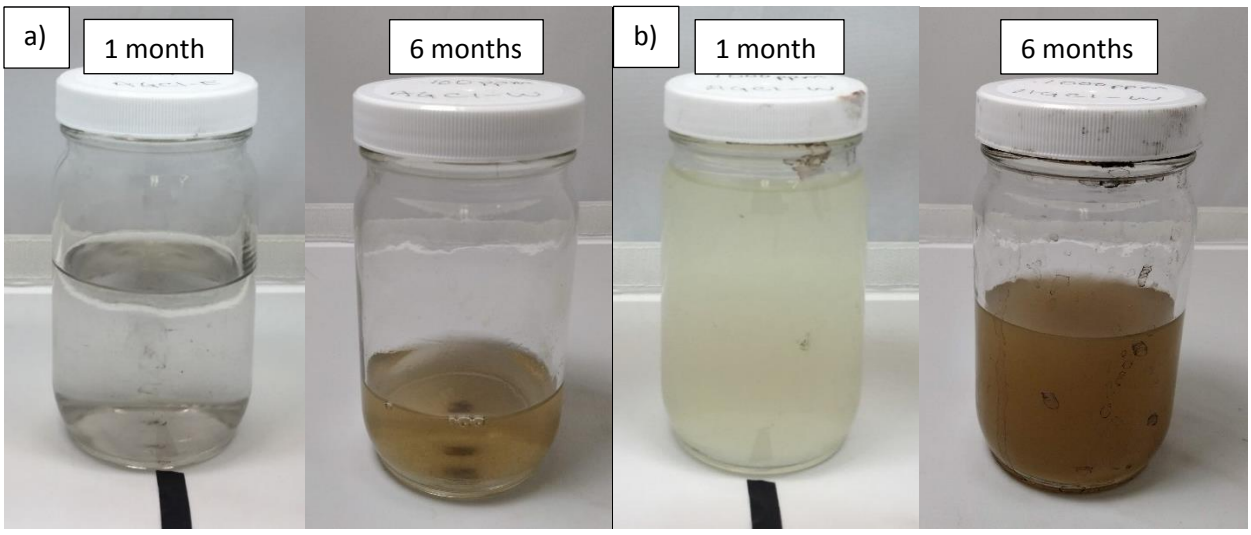

Figure 9 SOSs after room temperature storage for a) 100 ppm and b) 1000 ppm Ag formulations.

Silver concentrations were measured after 1 and 6 months of storage via ICP-OES, plotted in Figure 10. Results show a 90 % loss of silver in the 100 ppm solution and a 72 % loss for the 1000 ppm solution after 6 months. Stability of the SOSs could be reduced from exposure to ambient light accelerating the

rate of precipitation. Silver complexes are known to be photosensitive, with photochemical reactions in silver halide crystals being the basis for photography. The solubility of silver organometallics therefore can be improved by isolation from external light or with the addition of chemical stabilizing agents.

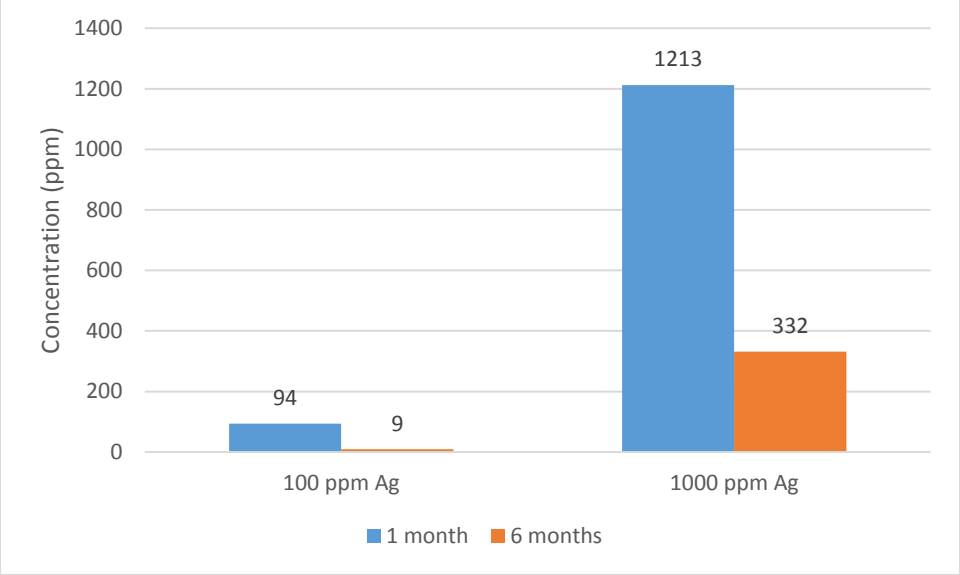

Figure 10 Silver drop out over a period of 6 months for formulations at 100 and 1000 ppm Ag. Measured via ICP-OES (Department of Chemical Engineering).

2.5.2 ICP-OES Analysis of Silver Organometallic on Fabric

ICP-OES analysis was performed on cotton fabrics treated with the primary water-based 100 ppm SOS to determine the amount of silver adhered to fibers during application. Samples were prepared in 10 mm petri dishes to ensure complete soakage of cotton fabrics (cut to the same size). High and low SOS volumes of 10 and 5 mL, respectively, were applied to represent various levels of spray loading—results given in Table 4. Measurement via ICP-OES requires aqueous samples, and so silver must be stripped from the fabric in order to determine concentrations. Treated fabrics were digested in 50 mL of a 60 % nitric acid-water solution for 24 hours and then boiled for an additional hour at 90 °C. Solutions were syringe filtered prior to ICP analysis to remove any partially digested cloth from samples.

Table 4 Concentration of silver on cotton fabrics measured via ICP-OES.

Applied Volume	Low (5 mL)	High (10 mL)	Control
Average Concentration (ppm)	4.41	11.89	0.50
Expected Concentration (ppm)	10	20	0
Percent Difference	44 %	59 %	High

ICP-OES results show significant amounts of silver recovered from cotton fabrics, with an average of 51 % of the expected value measured. Partial loss of silver can be attributed to the excessive amounts of organometallic solution applied to fabrics, which tended to pool in the petri dish. Examination of plates after drying show distinctive streak marks evident of residual silver. In addition, loss of silver could have resulted from incomplete recovery during acid digestion. Additional samples prepared without acid boiling showed near zero levels of silver, indicating the necessity for a hot digestive step. To improve recovery of silver from fabric in future studies, microwave digestion is recommended with additional digestion in hydrogen peroxide to completely dissolve fabric samples. Results on fabric provide further evidence for the strong adhesive properties of the SOS to organic fibers.

Chapter 3 | Colour Staining Metric on Fabric

This chapter discusses the development of methods for quantitative measurement of discolouration on stained fabrics treated with SOSs. An introduction describing the anatomy and function of colour vision is presented in Section 3.1 in support of methods in Section 3.3. Subsequent sections 3.2 and 3.3 detail the iterative design of test methods used to measure colour difference on silver treated fabrics.

3.1 Colour Science Introduction

3.1.1 Human Visual Perception

The perception of light and colour by the human eye is a physiological response involving a combination of photochemical and neural processes. Colour recognition is based on the transduction of incident photons into electrochemical signals that are then processed in the brain. An anatomical structure of the human eye is given in Figure 11. The eye is protected by the sclera, a white fibrous layer continuous with the cornea, the opening of the eye. Light entering the cornea is focused by the lens and imaged onto the retinal layer at the back of the eye. On the retina exists a small area near the optic nerve known as the fovea with the greatest acuity of vision.

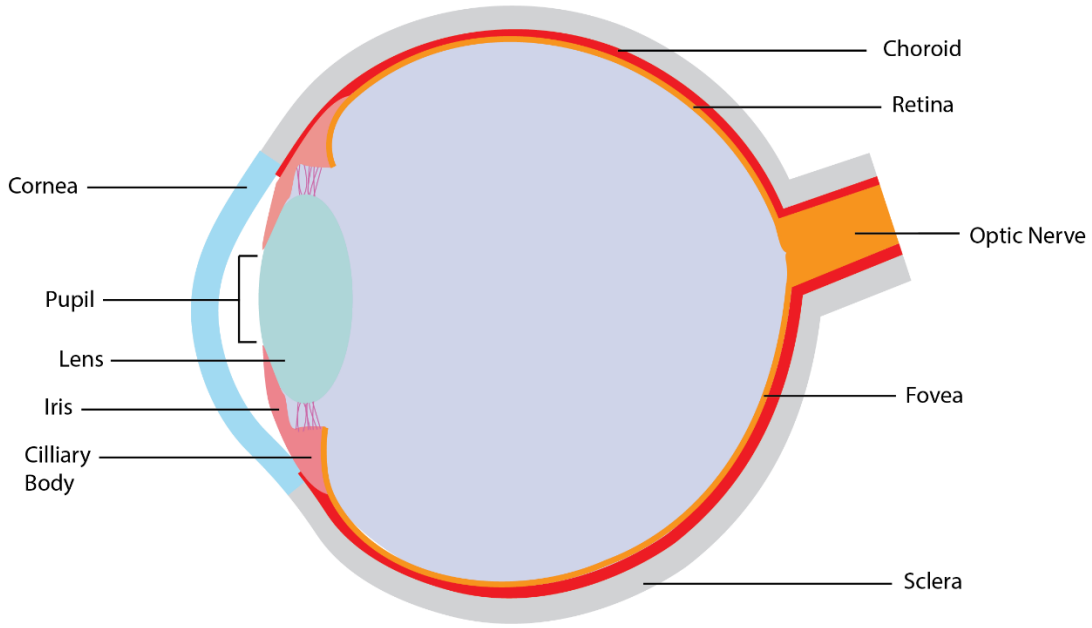

Figure 11 Anatomical diagram of the human eye, reproduced from [27].

Within the retina exist photoreceptors cells that chemically respond to light. For vertebrates these are rod cells, applied in low-light situations, and cone cells, used for bright colour vision—see Figure 12. The photoreceptors are located at the exterior of the retina, closer to the sclera, requiring light to travel the entire length of the retina to reach the light sensitive cells. Photoreceptor cells contain a type of protein molecule known as opsins embedded in disc structures within the outer segment of the cell. These proteins are responsible for the conversion of photons into electrical signals that travel through the optic nerve to the visual cortex to be processed—known as visual phototransduction.

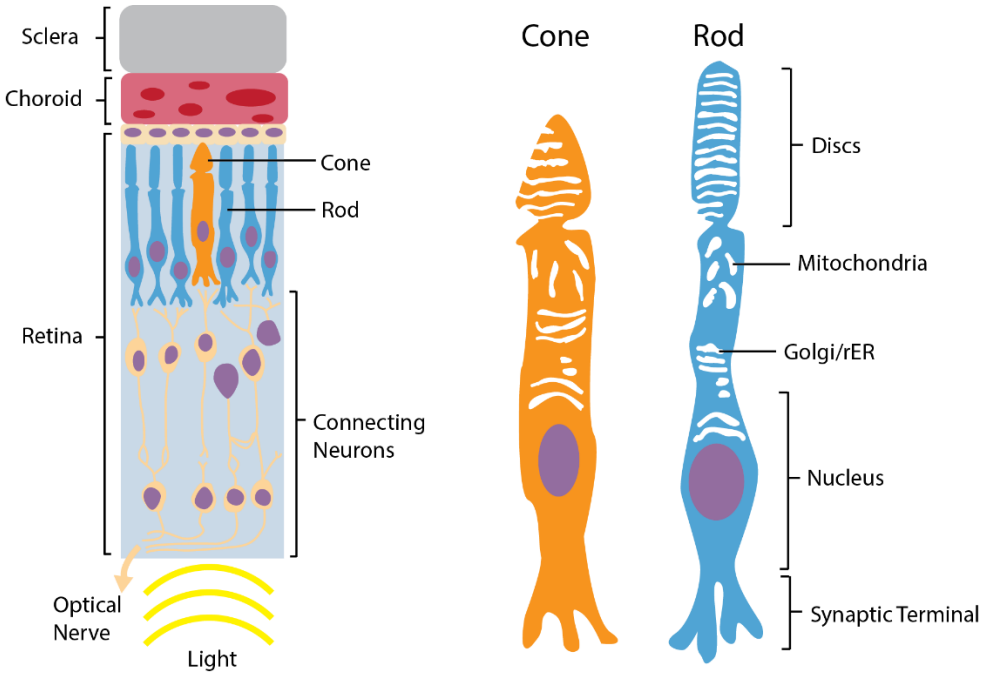

Figure 12 Structure of the retina (light enters from below) and photoreceptor cells in humans, reproduced from [27].

The first ever opsin was discovered in 1876, known as Rhodopsin, an extremely light-sensitive receptor protein found within rod cells. Rhodoposin is a member of a wider family of opsins, with another group—photopsins—being responsible for coloured vision in cone cells. As observed from the photoreceptor anatomies in Figure 12, the outer segment structure is larger for rod cells indicating an increased presence of opsin proteins. Rod cells thus have a higher sensitivity to light, supporting their application in low-light conditions.

Opsin proteins act as light receptors and function similar to the more general class of receptor proteins known as guanine nucleotide-binding protein-coupled receptors (GPCR). GPCRs are transmembrane units that act as intermediaries between the inside and outside of a cell, transmitting and amplifying extracellular signal messages (see Figure 13). The extracellular side of a GPCR is structured to receive a ligand molecule—much like a lock and key. Externally induced sensory stimulus triggers the production of the signaling ligand to concentrate outside the cell and bind to neighboring GPCRs. Reception of the ligand causes a conformational change to the structure of the GPCR, a physical change to the overall macromolecule shape. On the inside of the cell the GPCR is coupled to G-proteins—designated alpha, beta and gamma—that each activate their own respective intracellular functions. Guanine diphosphate (GPD) is bound to the G-alpha protein which in turn binds the G-beta gamma sub-units together to form a single complex; GDP-bound alpha represents the “off” state in an unstimulated receptor. Conformational change to the GPCR via receptor stimulation activates the G-alpha protein to bind GTP in place of GDP, representing an “on” state. GTP has a lower affinity for bonding and so disassociates from both the GPCR and the other G-beta gamma proteins. The dissociated G-proteins can diffuse through the membrane to bind onto effector sites, additional transmembrane proteins that generate secondary messengers and amplify the original extracellular signal [28].

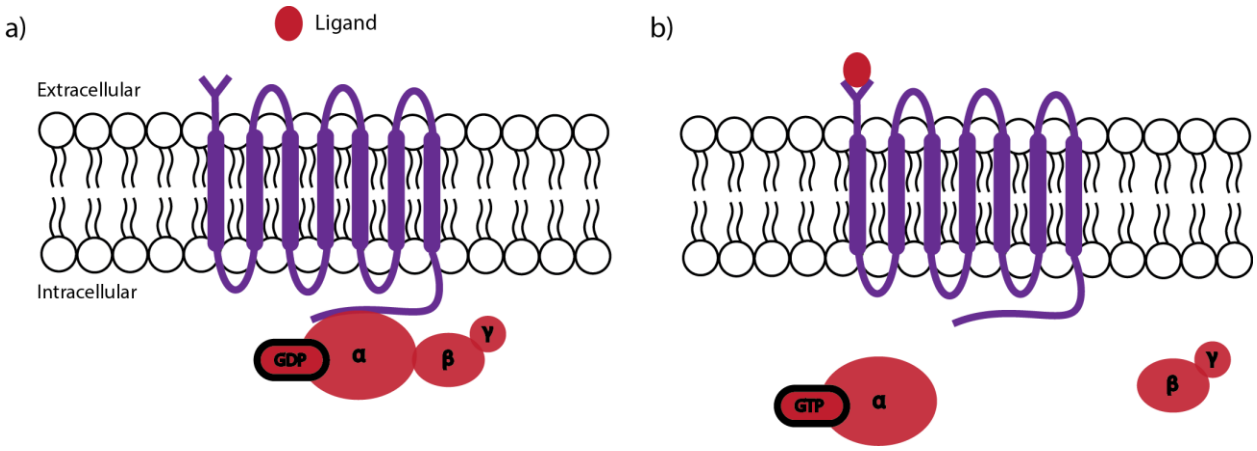

Figure 13 (a) An un-activated GPCR (purple) located within the cell membrane and (b) activation by an external signaling ligand that cause the release of coupled G-proteins inside the cell in an amplified response, reproduced from [28].

Visual opsins are structured similarly, consisting of two sub-structures: the primary GPCR structure known as scotopsin, and a covalently bound cofactor, retinal, that sits in a pocket of the scotopsin. The activating signal ligand in this case are photons of light that reach the retinal layer. Incident photons at specific wavelengths cause delocalized π-electrons within the retinal molecule to enter an excited state, changing the molecular bonding shape of retinal into a straighten configuration—the 11-cis-retinal structure isomerizes to all-trans retinal. Shape transformation of the retinal molecule pushes the scotopsin protein, causing a conformational change to the GPCR. Associated G-proteins becomes activated, Transducin, which eventually triggers the production of the secondary messenger cyclic guanosine monophosphate (cGMP) [29]. It is by this process that a photonic signal is transduced into an electrical-chemical signal. The absorbance spectrum of the retinal chromophore is largely dependent on the bonded opsin protein, i.e. different retinal-opsin complexes absorb photons of different wavelengths. The human eye contains a total of nine opsins used in both visual and non-visual functions, see Table 5.

Table 5 List of visual opsins and their functions in humans [29]

Location	Opsin	Peak Wavelength (nm)	Function
cone cells	long-wavelength, photopsin I	560	red colour vision
	middle-wavelength, photopsin II	530	green colour vision
	short-wavelength, photopsin III	420	blue colour vision
rod cells	rhodopsin	498	black and white vision, night vision
photosensitive ganglion cells	melanopsin	479	brightness, day and night cycles

Three coloured opsins—photopsins—are expressed in cone cells and form the basis of colour vision: a long-wavelength opsin sensitive in the yellow-green region, a middle-wavelength opsin sensitive in the green region, and a short-wavelength opsin sensitive in the blue region of the electromagnetic spectrum. Figure 14 illustrates spectral absorbance diagrams for the three variations of photopsins and rhodopsin.

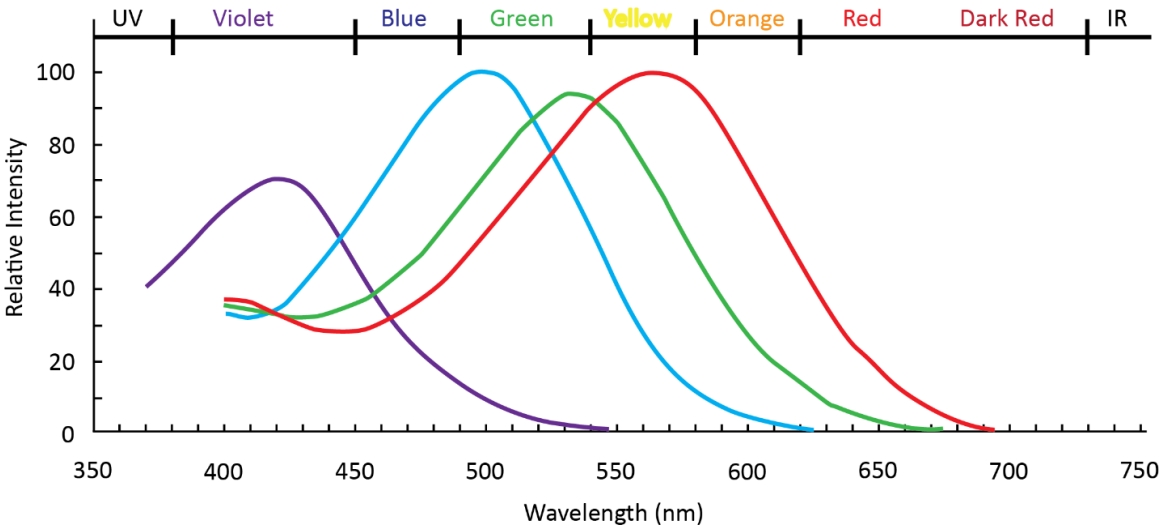

Figure 14 Absorbance spectra of visual opsins contained in rod and cone cells, reproduced from [30].

Human perception of colour is thus largely influenced by the absorbance spectra of individually stimulated photoreceptor cells. A visual field produced by light of many different wavelengths is attuned to the sensitivities shown in Figure 14. Therefore, a metric that quantifies the degree of staining on fabric should consider the mechanics of subjective human visual perceptions in its design.

3.1.2 Colourimetry Theory

Colourimetry is the science of defining the physical human perception of colour. The International Commission on Illumination (CIE) is a non-governmental organization based in Vienna, Austria responsible for international recommendations in photometry and colorimetry. Section 3.3 utilizes the CIE LAB colour space, a unique system designed with the consideration of human visual perception in the organization of its colours. The CIE LAB system attempts to establish a relationship between the spectral power distribution of visible light and the physiologically perceived colours registered by retinal photoreceptors. This section discusses the development and design behind the CIE LAB system.

Natural light is composed of many individual wavelengths in superposition. The range of visible light perceptible by humans have been historically defined by mathematical models, where colours are typically represented by a set of tuple primaries—e.g. RGB and CMYK. Similarly, in CIE LAB convention colours are defined by three unique values, given in Table 6. The CIE LAB system is structured such that a numerical difference between two colour values represents a proportional degree in perceivable colour difference by the human visual system.

Table 6 CIE LAB colour values

CIE LAB Value	Definition
L*	Lightness - black (0) to white (100)
a*	green (-) to red (+)
b*	blue (-) to yellow (+)

As discussed in the Section 3.1.1, human colour vision is comprised of signals produced from the stimulus of three distinct types of opsins in cone cells ranging in sensitivity—short, medium, and long EM wavelengths. Colour spaces defined by the spectral sensitivities of these three cones are known as LMS colour spaces, a foundation for CIE LAB.

Limitations with this system arise when distinguishing two very similar colours under certain lighting conditions, a phenomenon known as metamerism. The same LMS response can be obtained by multiple different spectral distributions based on specific wavelength activation of photoreceptors. Demonstrated in Figure 15, spectral distributions for two light beams (shown in black and grey) are overlaid on top of the LMS absorbance spectrums. Response of the medium cone cells to either spectral distributions results in the same degree of stimulation to the photoreceptor as both light beams have equal intensities but on opposing ends of the M cone sensitivity range. This effect is prevalent in optical illusions—e.g. the viral dress disputed to be blue and black, or white and gold.

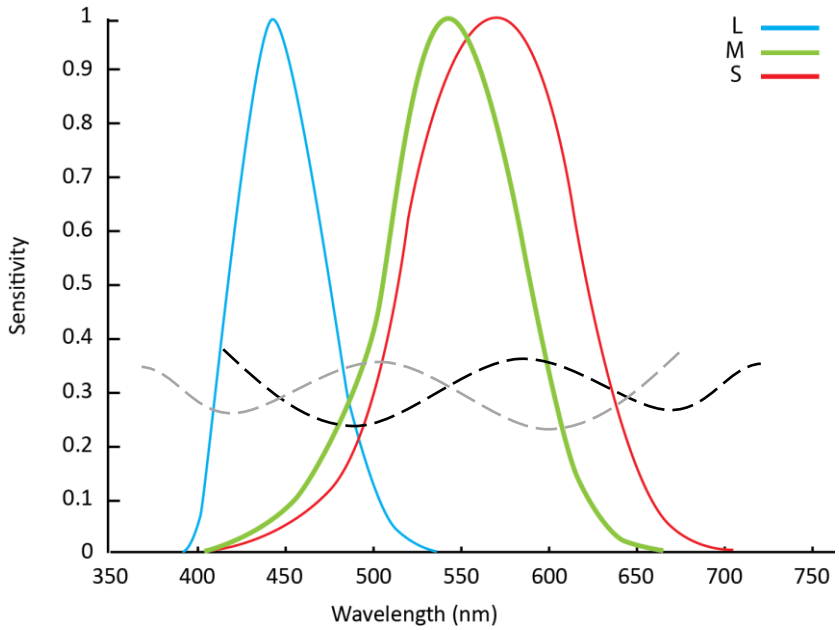

Figure 15 LMS cone response to two unique spectral distributions (black and grey). M cone response is the same for both light beams. Reproduced from [31].

Another visual phenomenon that results from the structure of the human eye is how light intensity affects the perception of colour. At lower intensities of light, rod cells dominate and no colour is observed. In bright light rod cells decrease in sensitivity and transfer visual function back to cone cells.

Due to this variation in sensitivities based on the active photoreceptor, the combined effect is that certain wavelengths of light appear to be brighter than others. Figure 16 illustrates the luminous efficiency function, V(λ), which describes the sensitivity of the human eye to different wavelengths of light. As an example, a laser at 450 nm would have to emit more power to be perceived as the same brightness as a laser emitting light at 550 nm wavelength.

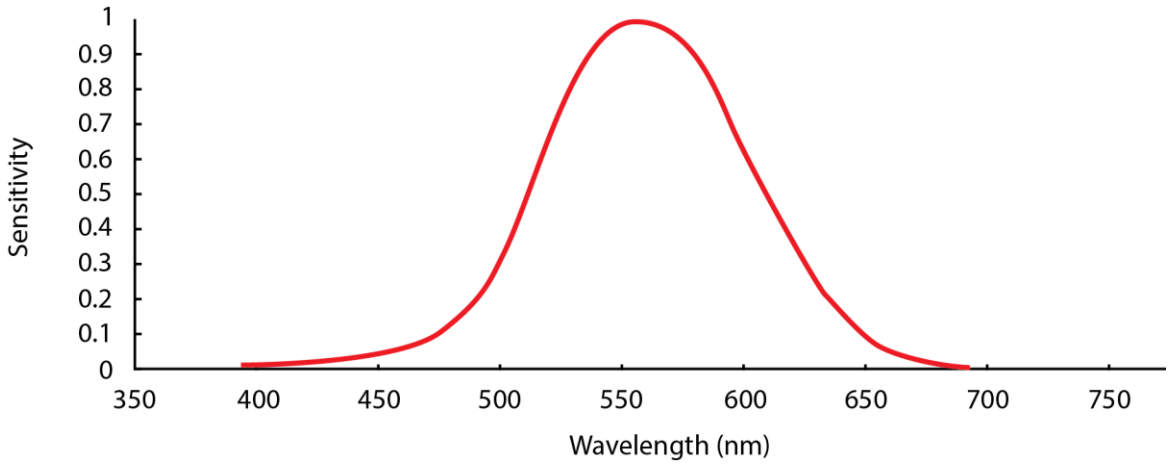

Figure 16 CIE luminous efficiency function, V(λ), plotting photoreceptor sensitivity for various wavelengths of visible lights, reproduced from [31].

In order to establish a method for differentiating colours LMS cone sensitivities were used to define the CIE 1931 colour matching functions. These functions express a founding principle of colour mixing, that any colour, X, can be made from the combination of three unique colours R, G, and B [32],

$$X = rR + gG + bB \tag{3.1}$$

Where r, g, and b are the intensity of the respective colours.

Single wavelengths of light at 700 nm, 546.1 nm and 435.8 nm were selected as the primaries for the R, G, and B color values, also known as tristimulus values. The functions were experimentally developed by having observers match a reference light by adjusting the intensity of three overlaid primary lights (R, G, and B). Colour matching functions r(λ), g(λ) and b(λ) were obtained by performing this match for every reference wavelength of light, shown in Figure 17. Looking at the r(λ) function, it can be observed that certain wavelengths of light require negative red luminosity values, e.g. at 520 nm. The physical interpretation is that these wavelengths of light could not be reproduced purely by adjusting the power of the primary lights and instead required adding the negative primary colour to the reference light. Perception of a reference colour is largely subjective and can change with variations in light, viewing angle, and field of view. To eliminate this variability a standard observer was established. The CIE 10-degree standard observer was defined as a 10° field of view where light is imaged in a 10° arc onto the fovea—the retinal area containing the highest density of cone cells.

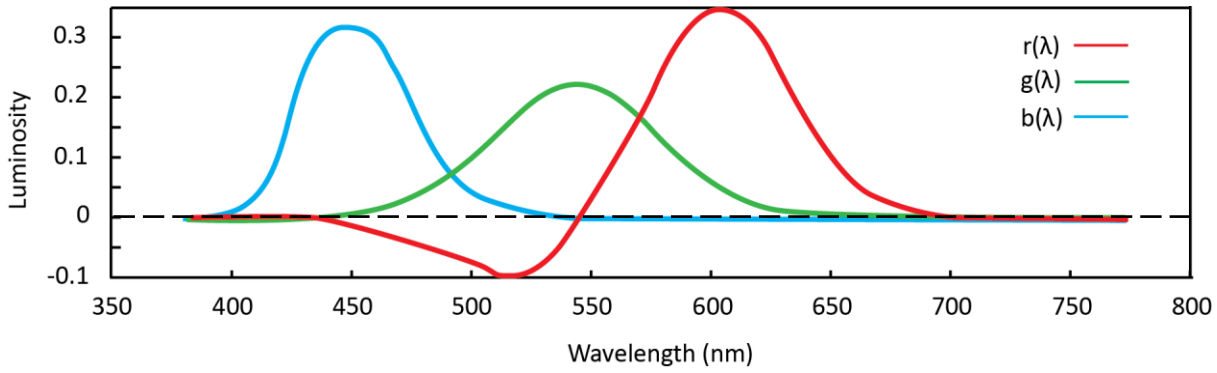

Figure 17 Colour matching functions, intensity of superimposed RGB lights required to match a reference wavelength of light, reproduced from [31].

Representing colours in this manner allows vector analysis to be applied, where r, g, and b represent the components of a vector locating a colour, point X, in a 3D colour coordinate system. Note that doubling the intensity of components r, g and b doubles the length of the vector but results in the same color, only brighter. The system can therefore be simplified by reducing all colours to the same light intensity, projecting everything onto a single plane and generating the colour space given in Figure 18.

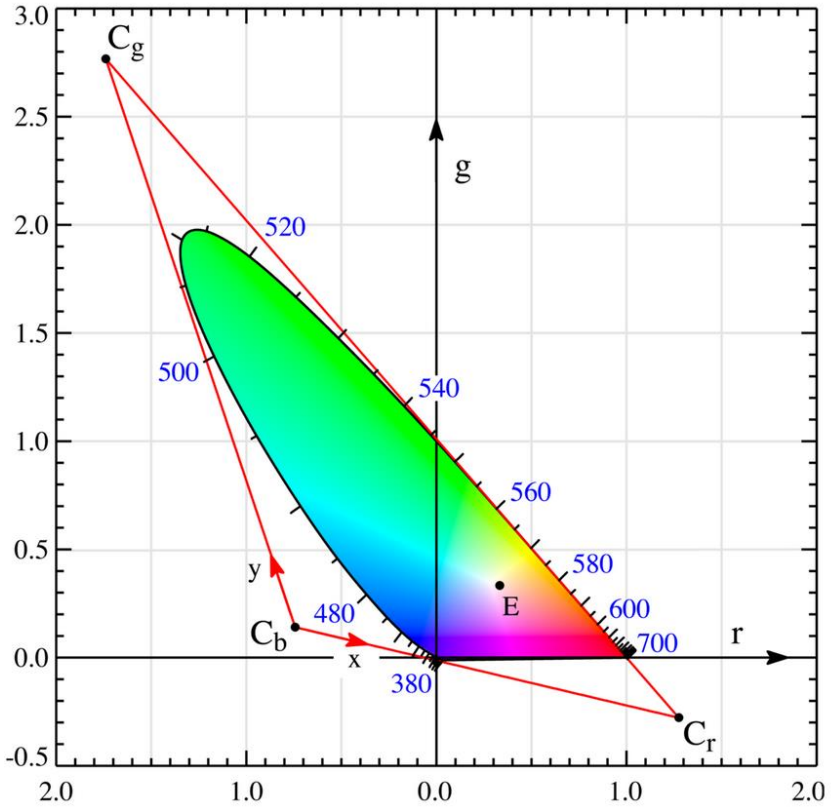

Figure 18 RGB colour space in a Cartesian coordinate system, with permission from [33].

Evolution to the CIE LAB system—and its precursor CIE XYZ—were attempts at simplifying the LMS tristimulus system, particularly regarding the complex numerical vector calculations performed on early computers. This was accomplished in two ways: first the colour matching function, b(λ), was transformed to match the luminous efficiency function shown in Figure 16. Colour brightness was therefore integrated with the colour matching functions themselves. A second linear transformation was then performed on the colour space itself to remove negative coordinates. Three new primaries X, Y, Z were selected as new system axes to which the rgb system was converted via a series of matrix transformations—this system is known as CIE XYZ. Coordinates X, Y, and Z exists outside the original rgb curve and therefore technically do not represent any physical colour.

The final set of transformations to the CIE LAB system were done to enable improved perceptual uniformity. Perceptual uniformity is the concept of quantitatively measuring perceived differences between two colours and equating that to a proportional distance in the coordinate system. Figure 19 illustrates this phenomenon on the XYZ colour space, where colours considered perceivably the same are circled. A perceptually uniform system would contain circles of all equal size, which is accomplished by additional transformations to the CIE LAB colour space.

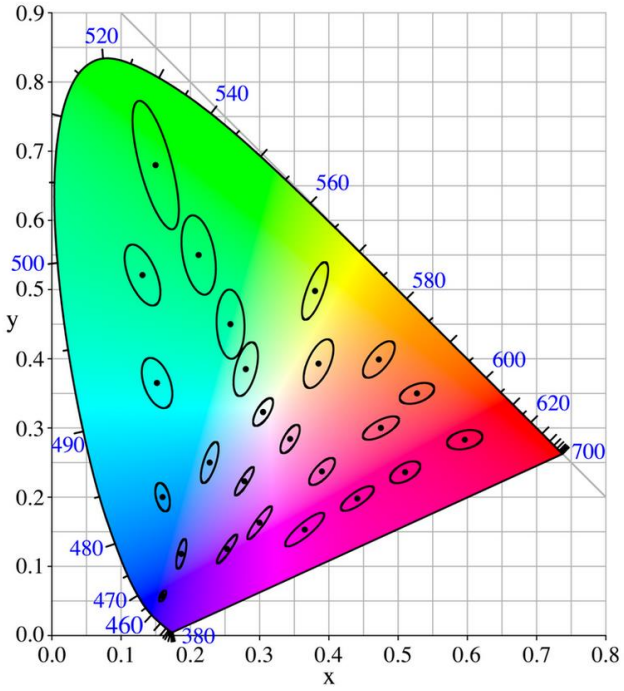

Figure 19 Perceptual uniformity on the XYZ colour space indicating the tolerance for similarly perceived colours, with permission from [33].

The CIE LAB system also defines the illumination of observed objects to standardize object reflectance and resolve the metamerism effect. For example, the common illuminant standard D65 corresponds to average daylight in Western/Northern Europe and is defined by the spectral power distribution shown in Figure 20.

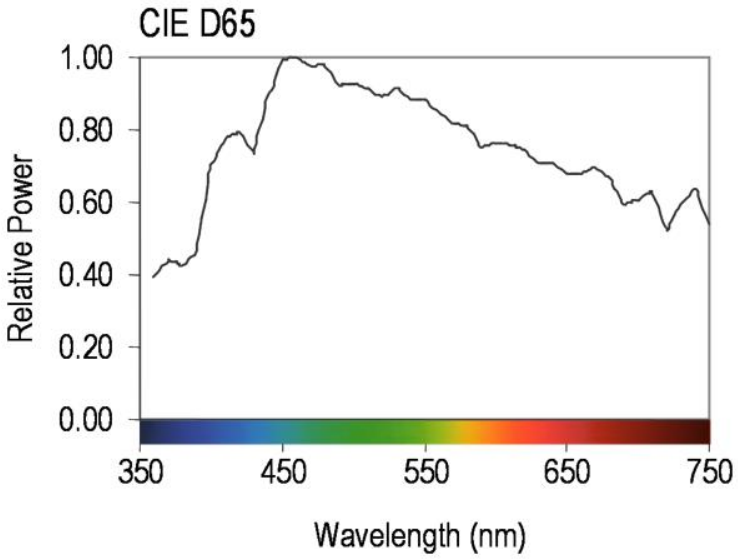

Figure 20 Spectral power distribution of D65 illuminant representing average daylight in Western/Northern Europe, with permission from [34].

Transformation to L*, a* and b* from CIE XYZ is as follows [35]:

$$L^* = 116f\left(\frac{Y}{Y_n}\right) - 16 \tag{3.2}$$

$$a^* = 500\left[f\left(\frac{X}{X_n}\right) - f\left(\frac{Y}{Y_n}\right)\right] \tag{3.3}$$

$$b^* = 200\left[f\left(\frac{Y}{Y_n}\right) - f\left(\frac{Z}{Z_n}\right)\right] \tag{3.4}$$

Where the n subscript denotes coordinates of the illuminant, for D65:

$$X_n = 95.0489$$

$$Y_n = 100$$

$$Z_n = 108.8840$$

The CIE LAB colour model is thus able to express colour difference by the Euclidean distance between respective L*, a* and b* coordinates, a metric known as Delta E (ΔE). The application to staining is evident in that visually perceived discoloring of fabrics can be quantitatively measured by calculating ΔE relative to a control.

3.1.3 Colour Difference Metric

Delta E is a quantitative measure of colour difference based on the distance between two CIE LAB colours. Values can range from 0 to 100, representing various degrees of physical human perception (see Table 7).

Table 7 Delta E human perception ranges [35]

Delta E	Visual Description
<= 1.0	not perceptible by human eyes.
1 - 2	perceptible through close observation.
2 - 10	perceptible at a glance.
11 - 49	colors are more similar than opposite
100	colors are exact opposite

The original formulation of Delta E was based on the Euclidean distance between colour values:

$$\Delta E^*_{ab} = \sqrt{(L^*_2 - L^*_1)^2 + (a^*_2 - a^*_1)^2 + (b^*_2 - b^*_1)^2} \tag{3.5}$$

The current Delta E 2000 formulation adds various weighting factors to correct for perceptual bias towards colour lightness, chroma and hue [35]:

$$\Delta E^*_{00} = \sqrt{\left(\frac{\Delta L'}{k_L S_L}\right)^2 + \left(\frac{\Delta C'}{k_C S_C}\right)^2 + \left(\frac{\Delta H'}{k_H S_H}\right)^2 + R_T \frac{\Delta C'}{k_C S_C}\frac{\Delta H'}{k_H S_H}} \tag{3.6}$$

Where,

$$\Delta L' = L^*_2 - L^*_1$$

$$\bar{C} = \frac{C^*_1 + C^*_2}{2}$$

$$a'_1 = a^*_1 + \frac{a^*_1}{2}\left(1 - \sqrt{\frac{\bar{C}^7}{\bar{C}^7 + 25^7}}\right)$$

$$a'_2 = a^*_2 + \frac{a^*_2}{2}\left(1 - \sqrt{\frac{\bar{C}^7}{\bar{C}^7 + 25^7}}\right)$$

$$\bar{C}' = \frac{C'_1 + C'_2}{2}$$

$$\Delta C' = C'_2 - C'_1 = \sqrt{{a'_1}^2 - {b^*_1}^2} - \sqrt{{a'_2}^2 - {b^*_2}^2}$$

$$h'_1 = \operatorname{atan}2(b^*_1, a'_1) \bmod 360°$$

$$h'_2 = \operatorname{atan}2(b^*_2, a'_2) \bmod 360°$$

$$\Delta h' = \begin{cases} h'_2 - h'_1 & |h'_1 - h'_2| \le 180° \\ h'_2 - h'_1 + 360° & |h'_1 - h'_2| > 180°, h'_2 \le h'_1 \\ h'_2 - h'_1 - 360° & |h'_1 - h'_2| > 180°, h'_2 > h'_1 \end{cases}$$

$$\Delta H' = 2\sqrt{C'_1 C'_2}\sin\left(\frac{\Delta h'}{2}\right)$$

$$\bar{H}' = \begin{cases} (h'_1 + h'_2 + 360°)/2 & |h'_1 - h'_2| > 180° \\ (h'_1 + h'_2)/2 & |h'_1 - h'_2| \le 180° \end{cases}$$

$$T = 1 - 0.17\cos(\bar{H}' - 30°) + 0.24\cos(2\bar{H}') + 0.32\cos(3\bar{H}' + 6°) - 0.20\cos(4\bar{H}' - 63°)$$

$$S_L = 1 + \frac{0.015(\bar{L} - 50)^2}{\sqrt{20 + (\bar{L} - 50)^2}} \qquad S_C = 1 + 0.045\bar{C}' \qquad S_H = 1 + 0.015\bar{C}'T$$

$$R_T = -2\sqrt{\frac{\bar{C}^7}{\bar{C}^7 + 25^7}}\sin\left[60° \cdot \exp\left(-\left[\frac{\bar{H}' - 275°}{25°}\right]^2\right)\right]$$

3.2 Pixel Shift Method

The scope of this section details a preliminary method to quantitively measure staining due to the application of SOSs on fabrics. Procedures for sample preparation described here are used in forwarding sections. Measurements are based on grayscale images of treated fabrics and their relative pixel intensity. This initial method does not consider human colour perception in its design. Methods established here are iterated upon in Section 3.3.

3.2.1 Fabric Sample Preparation

Procedures for sample preparation described here are used in forwarding sections. Treated samples were prepared from two commercial white knitted fabrics, organic cotton (Fabricland) and a synthetic polyester Coolmax (Invista). Varying concentrations of silver were applied to obtain up to 7 degrees of discolouration off-white. Two additional solvents, a 100 % and 50 % ethanol-based formulation, were tested to study the effects of evaporation. A complete design of experiment is outlined in Table 8.

Table 8 DOE of test samples treated with varying concentrations of silver and solvent bases, applied to cotton and Coolmax fabrics

Solvent Formulation	Ag Concentration (ppm)							
100 water	0	25	50	75	100	200	500	1000
100 ethanol	0	25	50	75	100	200	NA	1000
50/50 water-ethanol	0	25	NA	NA	100	NA	NA	1000

Sample fabrics were cut into 1” squares onto which 200 µL of organometallic solution was pipetted at the center and allowed to dry for 48 hours. Environmental temperature and humidity were monitored during the drying period to ensure consistent and repeatable application of the organometallic silver. Fluid movement through fibers and subsequent evaporation of the water and ethanol solvents affect the final discoloured stain. Maintaining a constant ambient condition was therefore critical to the development of a standardized measurement. Samples were dried on a Teflon surface to ensure complete absorption of the organometallic solution by the fabric.

Temperature and relative humidity were monitored using a HIH9130-021 model sensor produced by Honeywell International Inc., NJ, USA. The sensor is rated for a temperature operation range between 40 °C - 125 °C and 0 % - 100 % relative humidity. Figure 21 illustrates the sub-components of the system: the sensor chip is soldered to a dual inline package (DIP) and mounted to a PCB board that contains logic circuits for sensor conditioning and digital communication functions. Output signals are interfaced through an Arduino mini microcontroller and routed to a laptop PC to be post processed using MATLAB software.

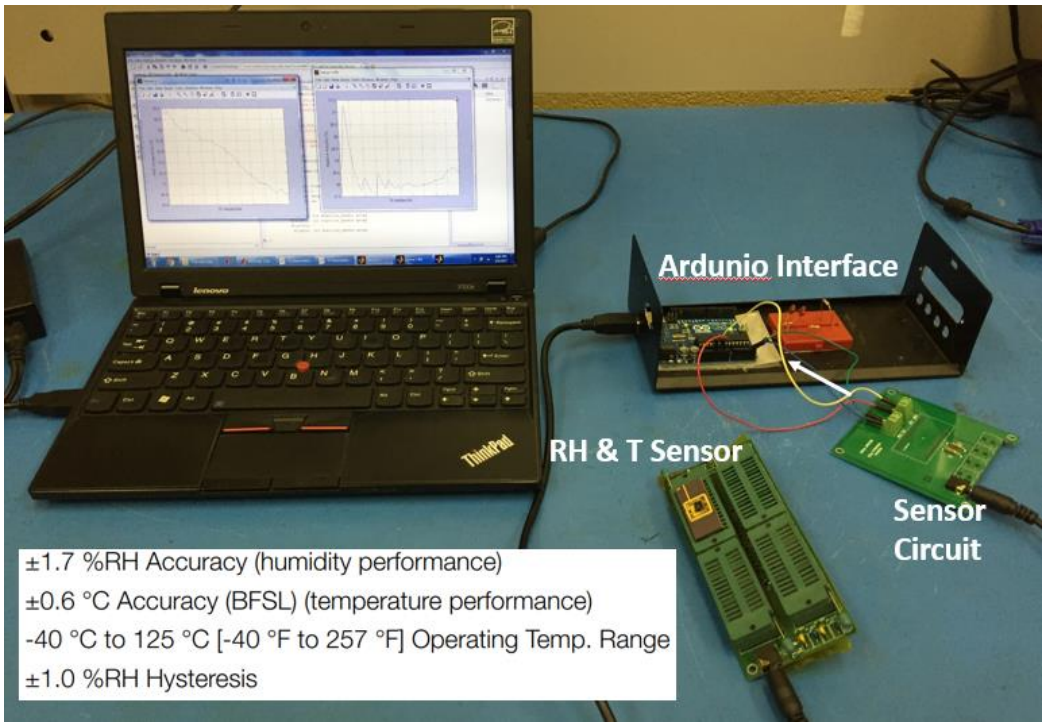

Figure 21 Temperature and relative humidity monitoring station (Electronics Lab E3 2118).

Drying for all fabric samples were maintained at an average ambient temperature of 24 °C and relative humidity of 48 %, example conditions plotted in Figure 22.

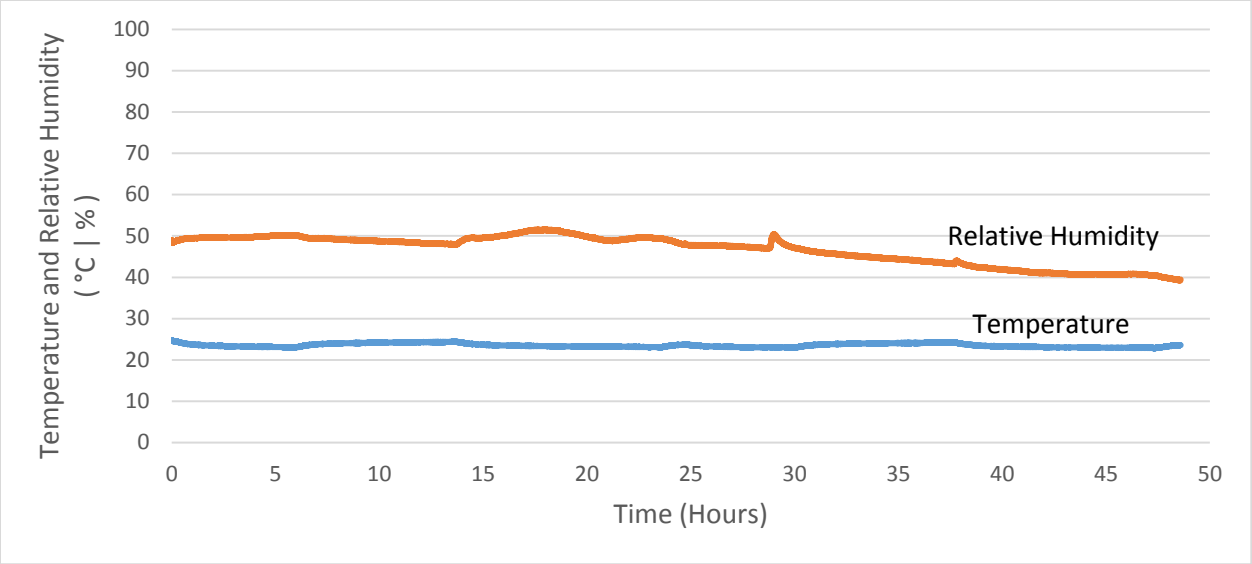

Figure 22 Temperature and relative humidity during a 2-day drying period for fabric samples.

2.2.3 Pixel Shift

Samples were set on white paper (CIE whiteness L* = 100, a* = b* = 0) and placed in a light tent illuminated using two 9W – 750 lumen fluorescent LED light bulbs, setup shown in Figure 23. A light tent was used to internally reflect light and attain a more even distribution of intensity and brightness.

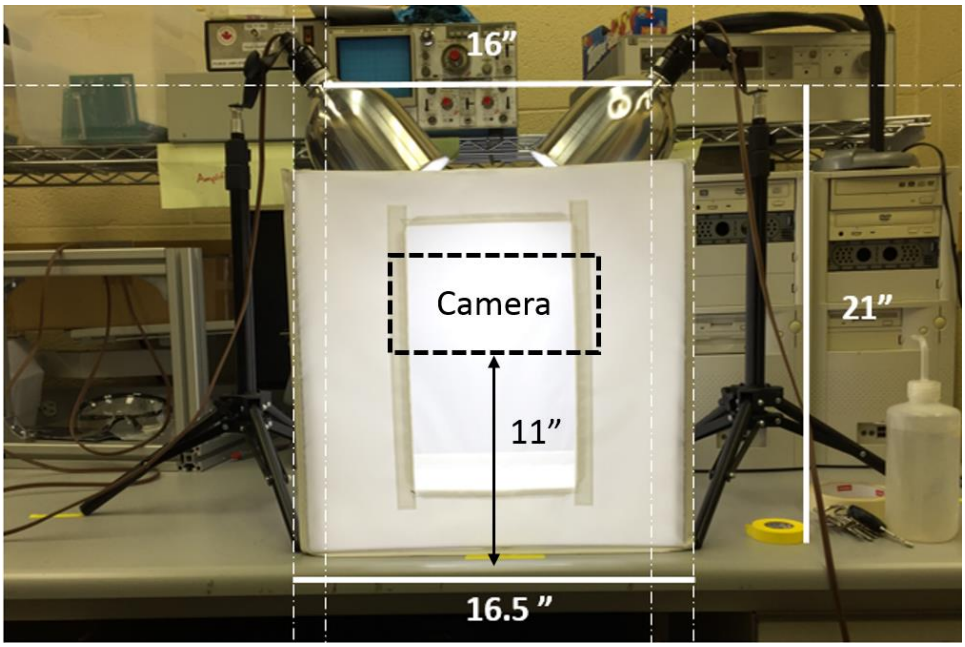

Figure 23 Light stage setup for pixel shift method.

Images of treated fabrics were taken using a Sony Alpha NEX-5 digital camera, and are presented for each solvent base in Figure 24 - Figure *26*.

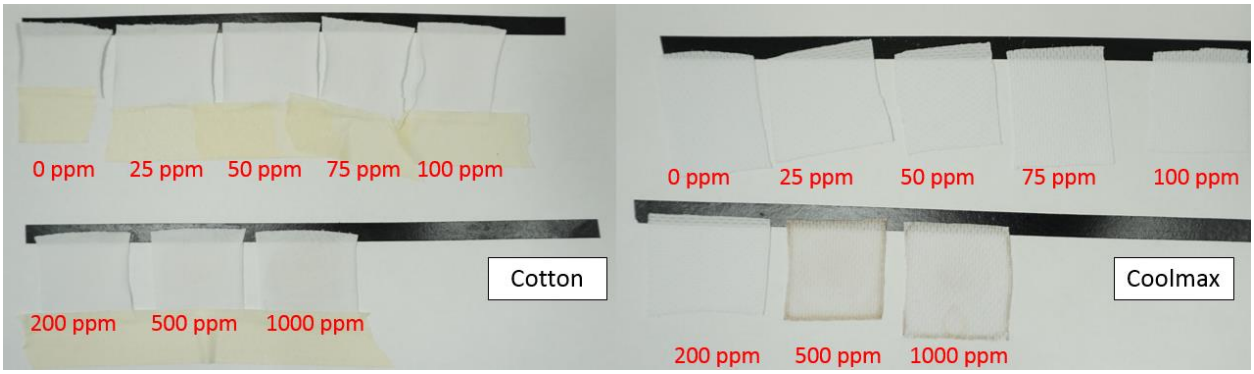

Figure 24 Water-based silver organometallic formulation at varying concentrations on cotton and Coolmax fabric.

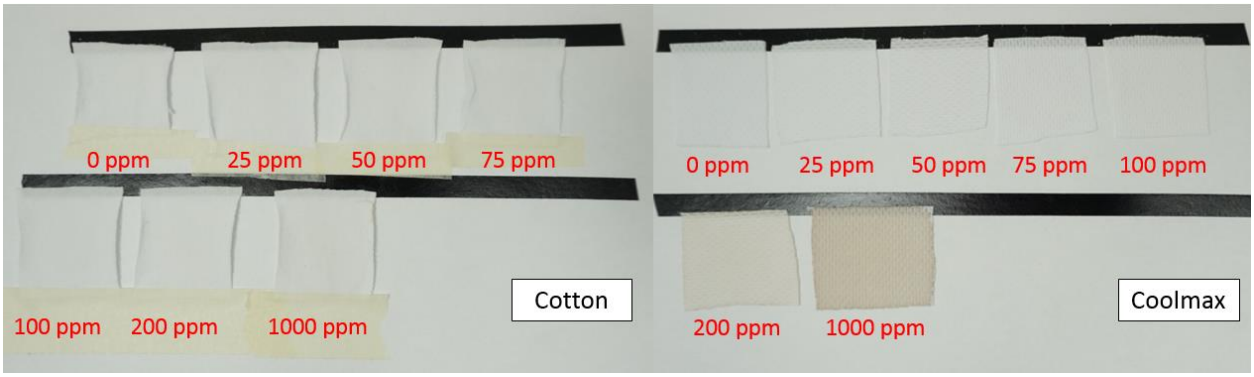

Figure 25 Ethanol-based silver organometallic formulation at varying concentrations on Coolmax and cotton fabric.

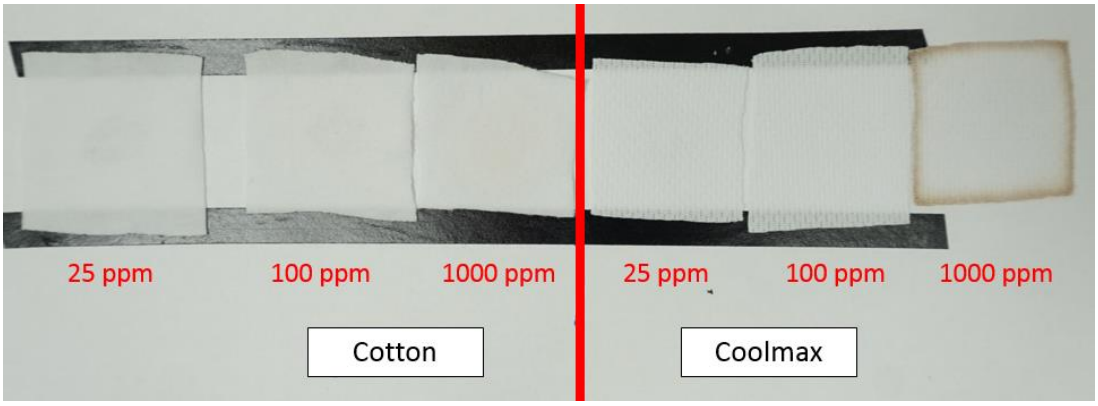

Figure 26 Water and ethanol-based silver organometallic formulation at varying concentrations on cotton and Coolmax fabric.

Standard RGB image files obtained from the camera were converted to greyscale and a perceptually uniform section of each fabric (250 x 250 pixels) was sampled using photo editing software GIMP—see Figure 27.

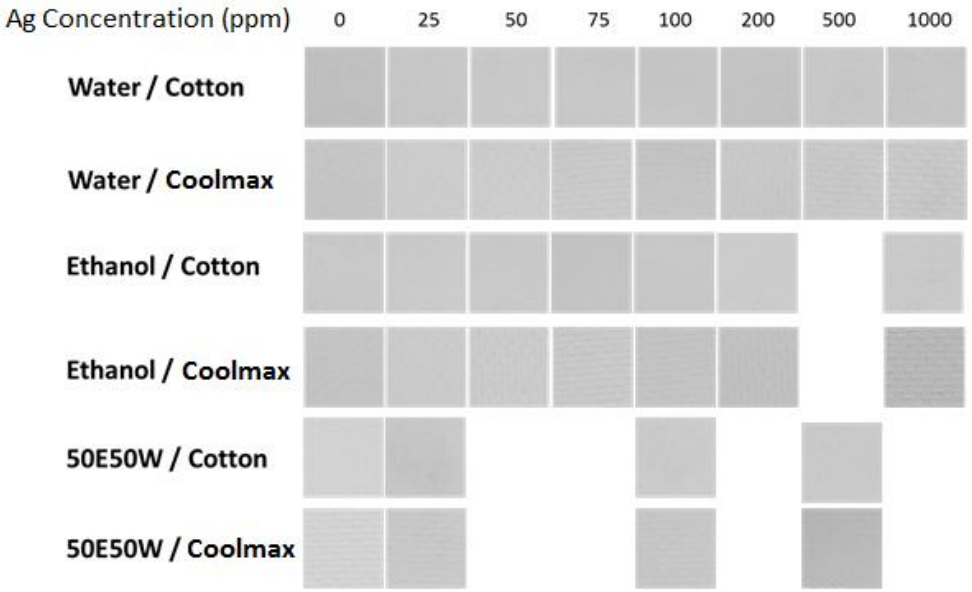

Figure 27 Greyscale images of treated fabric samples.

Images were processed in MATLAB to produce histogram plots indicating the distribution of tonal values for all 625,000 pixels. Figure 28 shows the image histogram for a fabric treated with 1000 ppm Ag next to a reference untreated cotton fabric. Quantitative colour differentiation is measured by calculating the difference between the peak of each normal distribution.

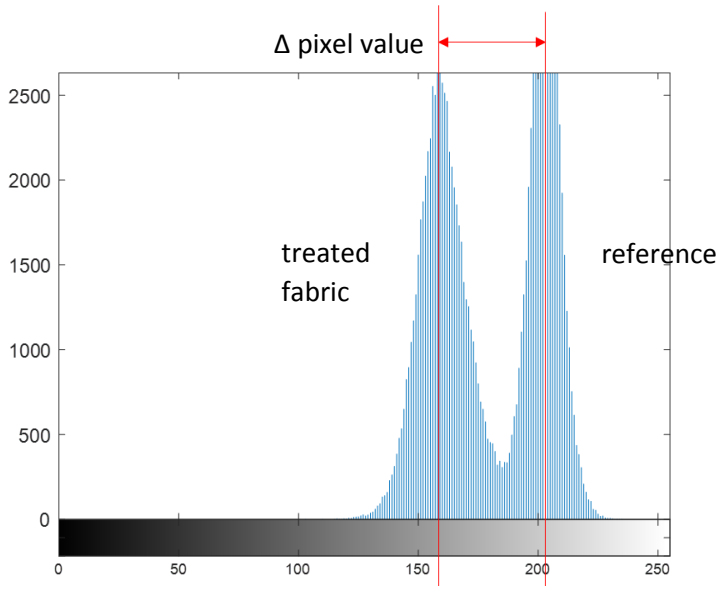

Figure 28 Greyscale image histogram of a treated fabric sample against an untreated reference.

2.2.4 Pixel Shift Results

Staining on treated fabrics was measured by the shift in average pixel value relative to an untreated reference. The resulting pixel shifts for increasing concentrations of silver is plotted in Figure 29 for each solvent and fabric combination (see Table 8).

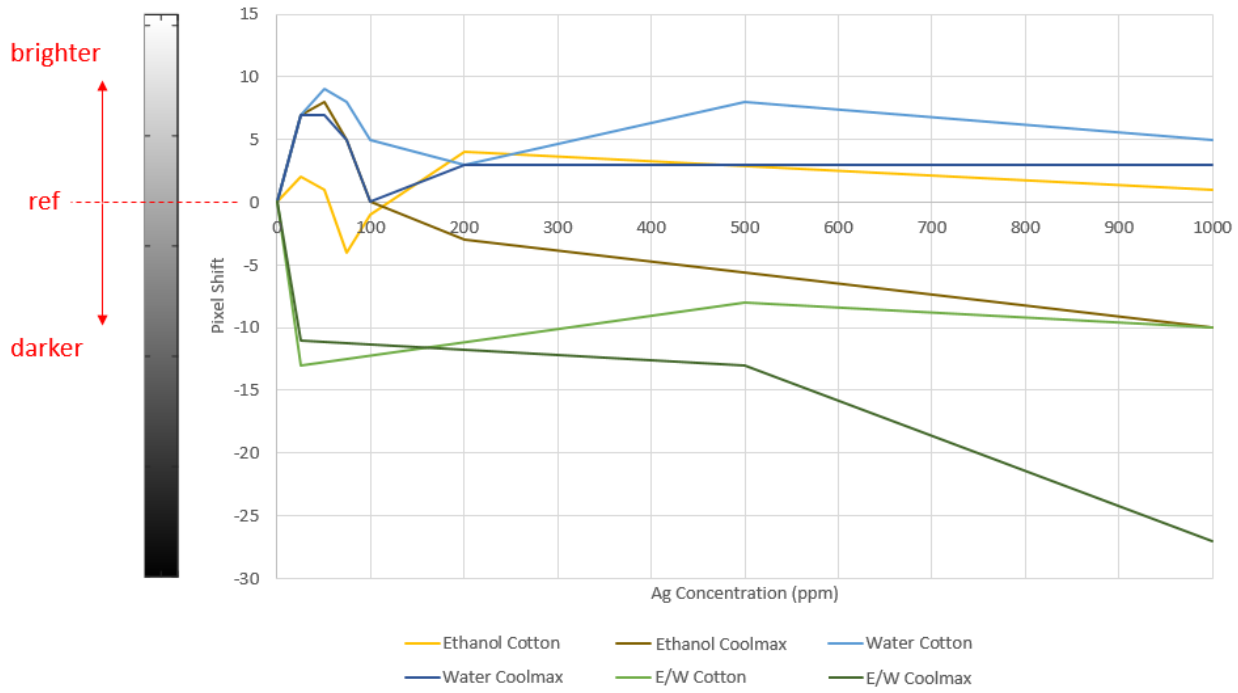

Figure 29 Pixel shift versus silver concentration for various fabric/formula combinations.

A systemic issue resulted in readings of lighter tones after fabric treatment as evident from the positive fluctuations in pixel shift. Analysis of the curves show that these fluctuations occur mostly in sets where minimal staining was observed at all concentrations of silver—i.e. the water-based formulations. The low degree of average pixel shift present in these cases allow sources of error to outweigh positive results.

Comparison of the original imaged fabrics (Figure 24 - Figure *26*) to the greyscale images in Figure 27 shows metamerism in effect, indicating the problem was a result of uneven stage lighting. Figure 30 shows a white point calibration preformed on the setup, were pixel shift was measured at different points on a solid white background. Preforming calculations relative to the center point, E, reveals that lighting was brightest near the center-top sections of the stage, with varying degrees of darkness at the other locations. Difficulties correcting this uneven stage light distribution necessitated a more enclosed design where illumination of the samples could be precisely controlled.

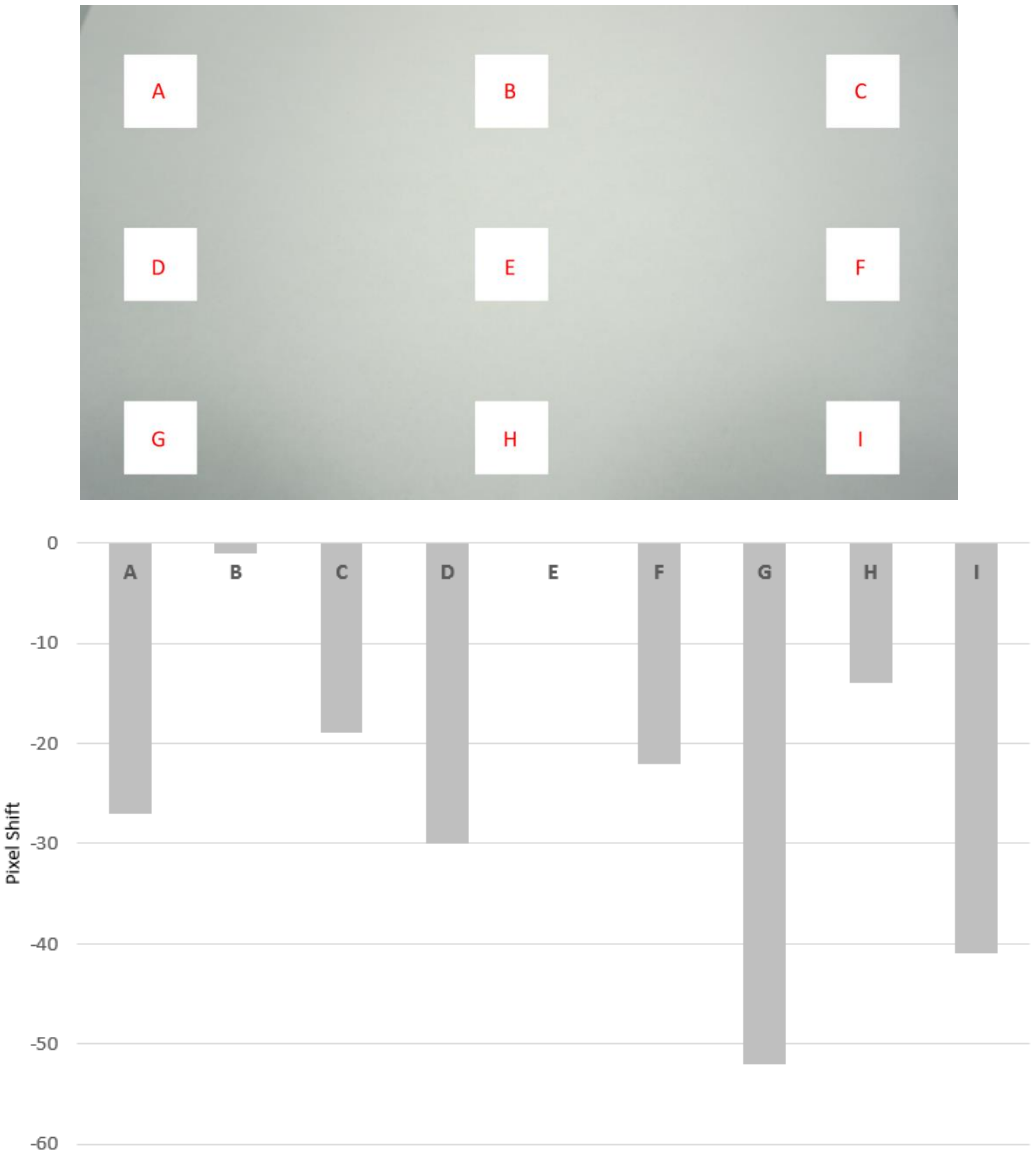

Figure 30 White point stage calibration of light tent relative to center point.

3.3 Nix Sensor Method

To correct for lighting inconsistencies associated with the pixel shift method a commercial spectrophotometer was tested for application to staining on fabrics, the Nix Pro Colour Sensor, Nix, Hamilton, Ontario, Canada. The sensor contains two high colour reproducing index LEDs at an illuminant/detector angle of 45° and 0° respectively and an aperture diameter of 0.6 inches—schematic given in Figure 31. Originally intended for use in architectural design and home decoration, the sensor possesses standardized features that make it suitable for measuring fabric discolouration. Specifically, the sensor is able to produce standard illuminants and is capable of measuring colour using the CIE LAB system. As discussed in Section 3.1, the CIE LAB system benefits from considering human colour perception in its assignment of colour values. Delta E ranges provided in Table 7 are used as reference to correlate quantitative measurements of fabric discolouration to qualitative descriptions of staining.

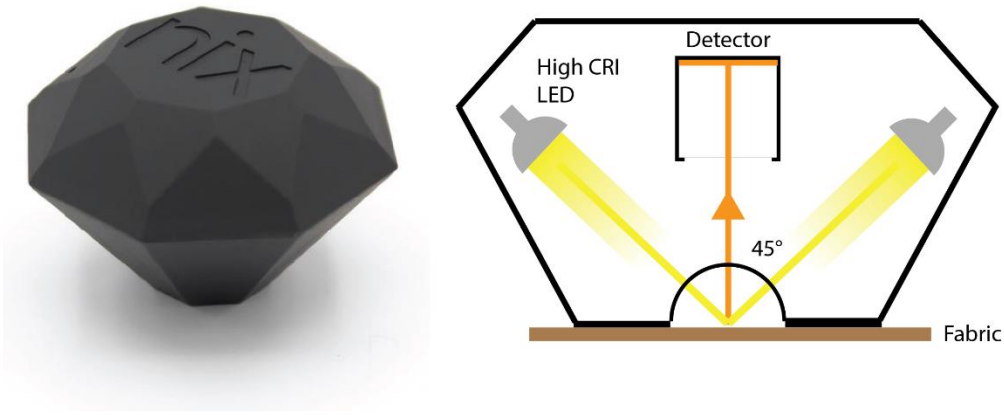

Figure 31 NIX Pro Colour Sensor diagram [36].

The NIX colour sensor was set to output the average of 10 repeated scans to monitor statistical variations. Mean and standard deviations are provided for two extreme staining conditions in Table 9. Initial results from colour sensor scans demonstrate a high degree of repeatability evident from the low standard deviation for all CIE LAB values.

Table 9 Statistical values for Nix Pro sensor measurements on heavy and light fabric stains.

Staining Concentration	Heavy Stain (1000 ppm Ag)			Light Stain (25 ppm Ag)		
Colour Values	brightness (L*)	green-red (a*)	blue-yellow (b*)	brightness (L*)	green-red (a*)	blue-yellow (b*)
Mean	85.77	-0.05	2.14	88.89	-0.32	-0.36
Standard Deviation	0.221	0.0972	0.5103	0.360	0.0422	0.0699

3.3.1 Nix Sensor Results

The same set of treated fabric samples outlined in Table 8 were tested again using the Nix Pro Sensor. Delta E values against increasing concentrations of silver organometallic for each respective solvent are given in Figure 32 - Figure *34*. The threshold for visually imperceptible colour change is marked in grey and termed the cutoff limit, indicating no visible staining.

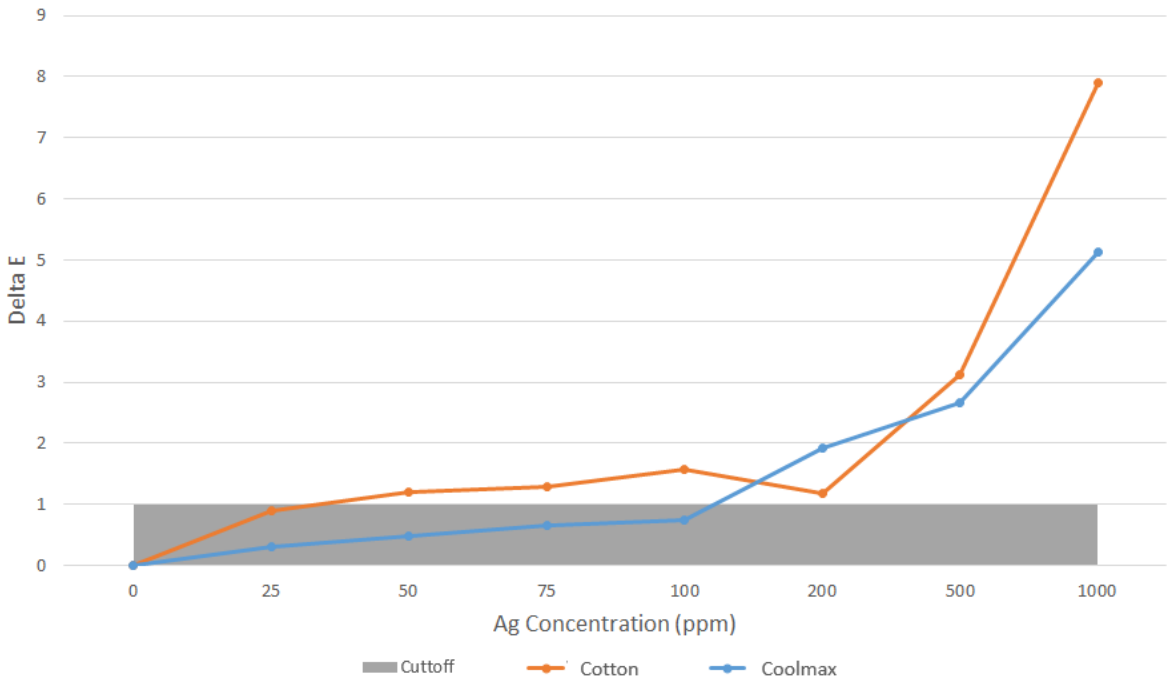

Figure 32 Delta E values for the quantification of the color difference against increasing concentrations of Ag for the water-based SOSs. Cutoff limit indicating imperceptible colour change.

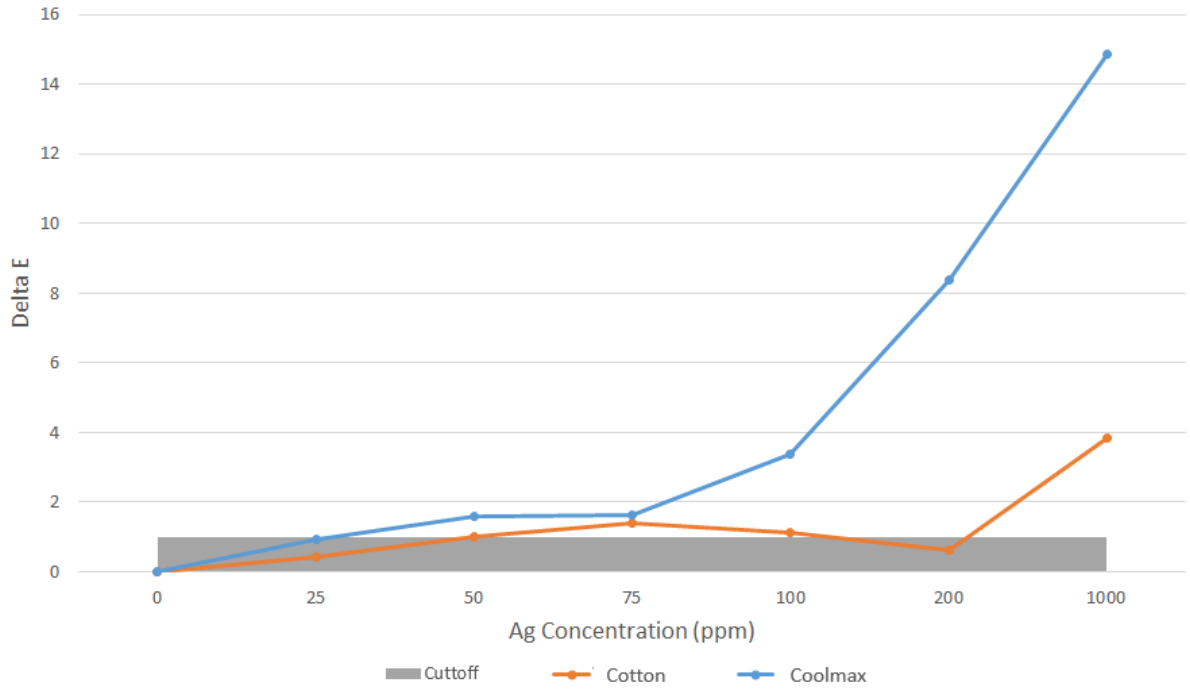

Figure 33 Delta E values for the quantification of the color difference against increasing concentrations of Ag for the ethanol-based SOSs. Cutoff limit indicating imperceptible colour change.

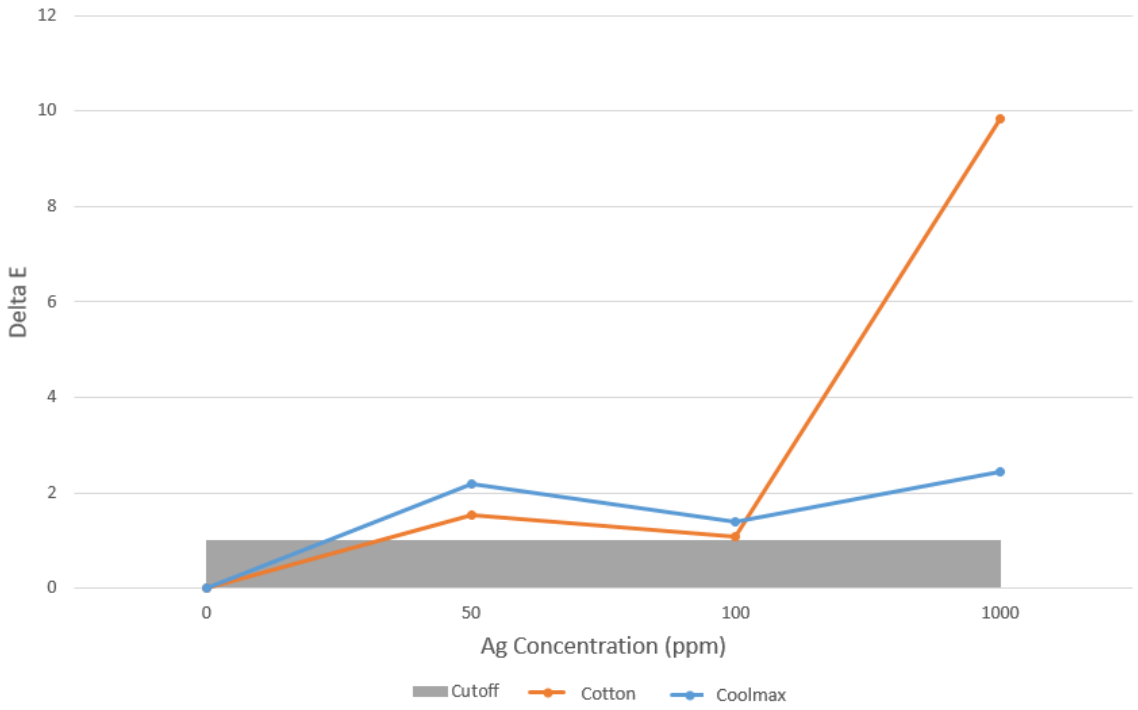

Figure 34 Delta E values for the quantification of the color difference against increasing concentrations of Ag for the ethanol-water-based SOSs. Cutoff limit indicating imperceptible colour change.

In general, colour sensor data correlated well with the physically observed discolouration on fabric. Evenly stained samples demonstrated an exponential increase in Delta E values (discolouration) with increasing concentrations of silver, most clearly observed in the ethanol-based formulations on Coolmax. As discussed in Section 3.1 this is the expected trend, as retinal sensitivity is a power function of light intensity following a logarithmic scale. Colour difference, which is largely influenced by perceived brightness, should therefore rise exponentially with increasing concentrations of silver.

Sensor measurements for water-based formulations on Coolmax fabric were the most inconsistent compared with visual observations due to uneven staining patterns developed after drying. Coolmax fabric is commonly used in athletic garments for its credited breathability, hydrophobic properties and strong ability to wick moisture. These properties arise from the cross section of Coolmax fibers, which—unlike the round fibers of cotton—are “peanut” shaped, creating channels capable of pumping fluid via capillary action. This pumping action effectively reduces the absorbency of the fiber and accelerates drying times compared to traditional cotton fabric. When applied onto Coolmax fabric the water-based organometallic solution is pumped outwards from the center, collecting silver at the edges of the square, and forming a gradient halo-like effect (see Figure 24). The aperture size of the Nix Pro colour sensor is fixed at 0.6 inches, resulting in scan area of 0.29 square inches. The sensor averages individual pixel values that comprise the overall scan and outputs a single CIE LAB colour. For gradient colouring on fabric the result is an apparent decrease in Delta E values at higher concentrations of silver, seen in Figure 32. In these cases, multiple scans must be performed across the fabric to properly measure overall average staining. Alternatively, fabric samples can be cut to match the aperture size of the sensor.

3.3.2 Colour Sensor for High Temperature Test

Discolouration was measured for samples dried at high temperatures to simulate application of SOS treated fabrics in standard home dryers. Fabrics were dried in an OMEGALUX LMF-3550 oven and operated on standard drying cycles—55 ± 5 °C for 30 minutes. Samples were prepared using methods in Section 3.2.1 from cotton fabrics treated with the primary water-based SOS, see Figure 35. Discolouration was monitored at 10-minute intervals using the Nix colour sensor. Delta E values for stains at each silver concentration was calculated relative to an untreated cotton and plotted in Figure 36.

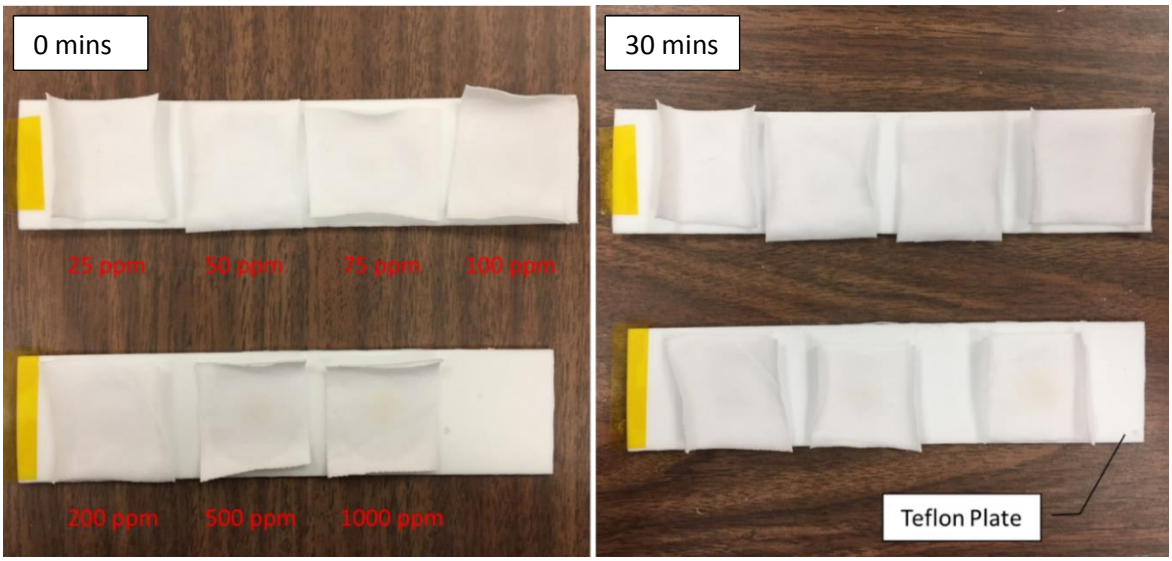

Figure 35 Cotton fabrics treated with 200 µL of SOSs at various Ag concentrations after drying at 55 °C.

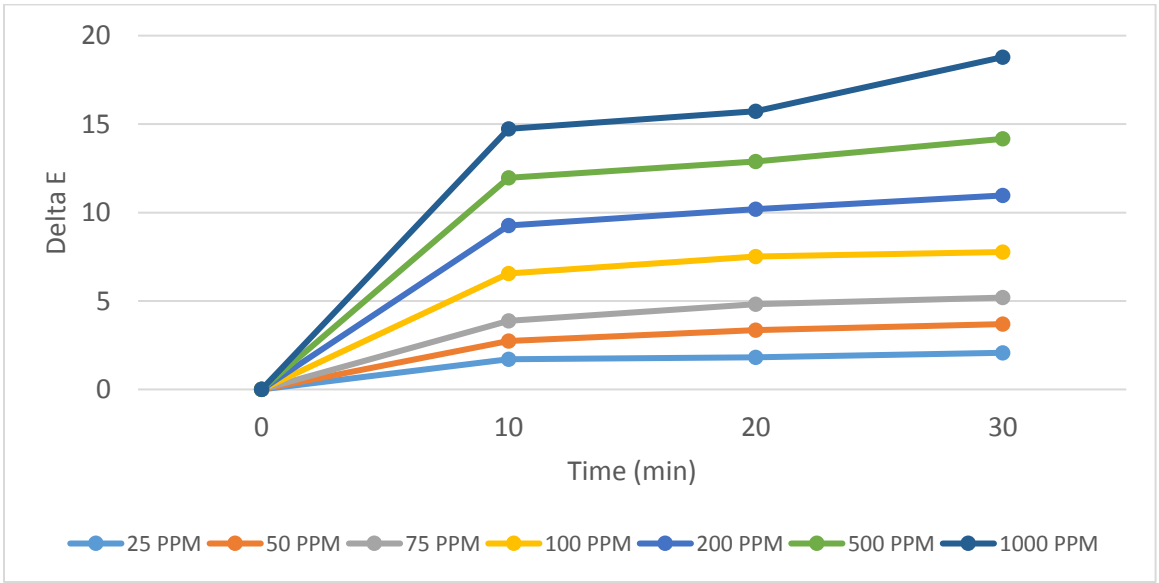

Figure 36 Delta E values for samples at increasing concentrations of Ag dried at high temperature.

Staining due to high temperature was significantly more pronounced. High temperature drying nearly doubled Delta E values at all concentrations compared to stains produced at room temperature. Explanation for increased staining observed at high temperature is likely due to the same mechanics that formed gradient stains in the water-based formulations on Coolmax fabric. Higher temperatures accelerate the rate of evaporation causing an increase in fluid flow towards free surfaces. The silver organometallic is carried outwards by the flowing water until it evaporates, depositing silver in higher concentration near the surface and resulting in a more prominent stain.

An additional test was performed at 130 ± 5 °C to verify this hypothesis, samples shown in Figure 37. At higher temperature staining becomes even more pronounced, with similar halo effects observed on cotton at 1000 ppm Ag to that on Coolmax fabric. The mechanism for staining at higher temperatures is therefore a consequence of increased rates of evaporation.

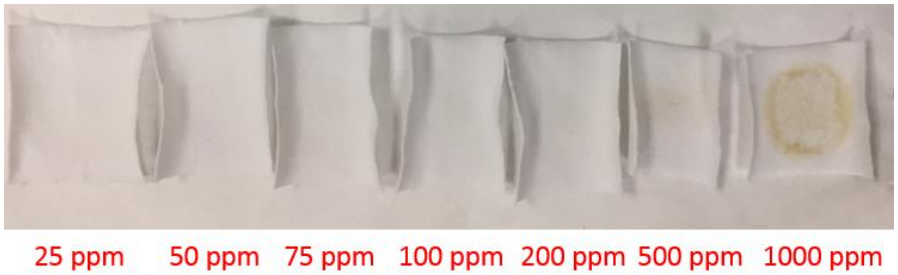

Figure 37 Stained cotton fabrics dried in an oven at 130 °C.

Chapter 4 | Antibacterial Efficacy Testing on Fabric Surfaces

The silver-based organometallic spray is a commercial product proposed for anti-odor treatment on fabrics. Antibacterial efficacy tests are critical to establishing scientific support behind manufacturing claims. Standardized test methods have been developed by various organizations to quantify the effectiveness of antimicrobial textiles against bacteria, including the American Association of Textile Chemists and Colorists (AATCC) and the American Society for Testing and Materials (ASTM). Evaluation of SOSs in this chapter are focused on the water-based formulations at 100 ppm (primary) and 1000 ppm (for comparison) silver. Section 4.1 evaluates antibacterial efficacy of the SOSs based on standardized test methods: disc diffusion method, colony formation and the minimum inhibitory concentration (MIC) assay. Section 4.2 presents the development of a proposed method based on concentration of bacterial ATP.

4.1 Standard Test Methods for Antibacterial Textiles

Experiments were performed in accordance to protocols established by the US Environmental Protection Agency (EPA), which applies regulatory standards used to define general antimicrobial surfaces [37]. Bacteria species, *Escherichia coli,* was chosen as the inoculum due to its standardized use, wide availability, and fast rate of reproduction. Antibacterial experiments were performed in biologically approved labs under Prof. Bill Anderson of the Chemical Engineering Department, University of Waterloo.

4.1.1 Disc Diffusion Method

This section assesses antibacterial efficacy of textile fabrics treated with the principal SOS using the disc diffusion method. Experiments were performed in accordance to standard protocols developed by the American Society for Microbiology [38]. Disc diffusion method, also known as the Kirby-Bauer test, measures the antibiotic resistance of bacteria based on the diffusion of an antimicrobial in an agar medium. Fabric discs treated with SOS are placed in contact with pre-inoculated agar. Water from the agar is absorbed into the disc, allowing silver to diffuse into the surrounding area—due to concentration gradients—and eliminating any contacting bacteria. The diffusion of silver continues at a decreasing logarithmic rate until a critical point is reached where the inhibitory effect of silver is overpowered by bacteria, forming a zone of inhibition around the disc. The area of this zone is used as a quantitative metric to correlate resistance of bacteria to the silver-based organometallic.

Disc diffusion method summarized as follows:

1. Discs (6 mm diameter) were stamped and treated with 30 µL of SOS and dried for 24 hours.
2. Plate count agar (PCA) was prepared to an average depth of 4 ± 1 mm. PCA composition consists of (w/v): pancreatic digest of casein 5g/L, yeast extract 2.5 g/L, dextrose 1 g/L, and agar 15 g/L
3. Inoculating bacteria, *Escherichia coli*, was cultured in lauryl sulphate broth (LSB) and diluted with a phosphate buffer solution (PBS) to an absorbance of 0.2 at 600 nm (OD_{600}) using a HP 8542A Diode Array Spectrophotometer. Optical density values represent an approximate bacteria concentration of 10^8 colony forming units per milliliter (CFU/mL), equivalent to the McFarland standard inoculum specified in the protocol.
4. Agar plates were inoculated with 100 µL of *Escherichia coli* (10^8 CFU/mL) and spread to create an even bacteria layer.
5. Plates were incubated for 24 hours at 38 °C to allow colony formation on agar.
6. Treated discs were placed on cultured agar plates and incubated for an additional 24 hours to allow for silver diffusion.
7. Plates were imaged and area of inhibition zones calculated.

The silver-based organometallic solution was tested at concentrations of 100 ppm and 1000 ppm Ag relative to an untreated control. Textile fibers, cotton and borosilicate glass, were used as disc substrates. Discs were tested in quadruplicate to determine statistical averages for zone areas. Imaged plates are presented in Figure 38 and Figure *39*, cotton and glass fiber substrates respectively.

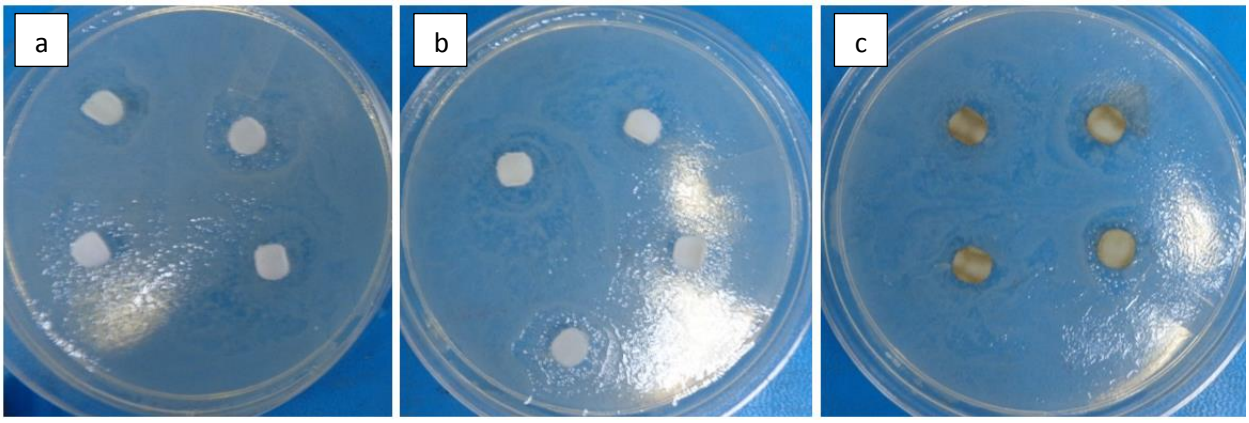

Figure 38 Cotton fabric discs 6 mm in diameter: a) control b) 100 ppm Ag and c) 1000 ppm Ag.

The diffusion of silver in the cotton samples produced unclear zones of inhibition, primarily due to poor contact with the agar surface as seen in Figure 38. Absorption of water from the agar medium caused the cotton fabrics to curl during incubation, reducing contact and preventing proper diffusion of silver. No visible stains were observed in the surrounding areas of the disc for either concentrations of silver, indicating a general lack of Ag diffusion into the agar medium. The disc diffusion method was thus determined to be unsuitable for absorbent organic fabrics such as cotton.

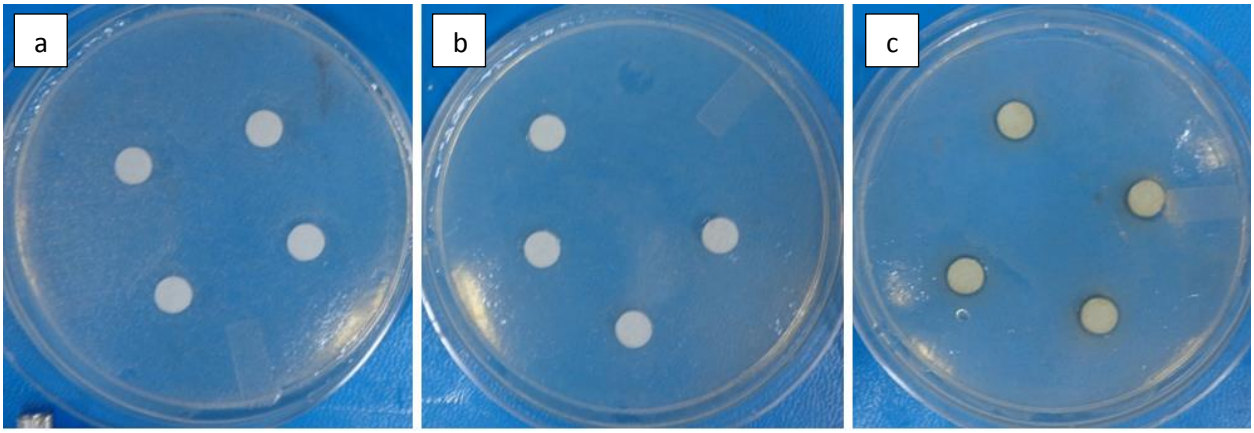

Figure 39 Borosilicate glass fiber discs 6 mm in diameter: a) control b) 100 ppm Ag and c) 1000 ppm Ag.

As a result of curling effects observed in cotton fabrics, disc diffusion testing was evaluated using standard filter paper substrates made from borosilicate glass fibers (Whatman, Maidstone, UK)—pore size 1.6 µm. Silver diffusion from the filter paper samples produced more distinct zones of inhibition, particularly at 1000 ppm Ag concentration where clear rings are visible in Figure 39 c) surrounding the treated discs. Diffusion of silver into agar was also evident by brown stains in the surrounding area. In contrast, samples at 100 ppm Ag showed little signs of silver diffusion with no discernible zone of inhibition—a similar result to the control sample. No correlation could therefore be established between bacterial resistance and the silver-based organometallic at such low concentrations.

Comparing disc substrates in Figure 38 and Figure *39*, the lack of silver diffusion observed in cotton samples could be attributed to the strong binding properties of the organometallic to organic fibers. Cotton samples at 1000 ppm Ag remained heavily stained even after incubation, indicating a majority of the silver remained adhered to the disc. In contrast, weaker bonds formed between the SOS and the chemically unreactive borosilicate glass fibers allowed for easier disassociation of silver particles from the disc and subsequent diffusion into agar. Results from the disc diffusion test provides further evidence of the durability of SOS on fabrics. Due to the poor compatibility with traditional textile garments no further testing was performed.

4.1.2 Colony Formation Method

This section assesses antibacterial efficacy of treated fabrics based on textile standards ASTM STP1558 [39], AATCC TM-100 [40] and silver antibacterial experiments performed by Wright et al. [41]. Viable bacteria recovered from treated fabrics are plated onto agar to allow for the proliferation of colonies. Log reductions are a determined as a quantitative metric for antibacterial activity based on the number of discrete colony forming units (CFU) present on plates after incubation. Log reductions are calculated relative to the initial bacteria count using,

$$R = -\log_{10}\left(\frac{C_{sample}}{C_{initial}}\right) \tag{4.1}$$

Equivalent percent reductions for log reductions of bacteria are provided in Table 10.

Table 10 Log reduction of bacteria to percent reduction

Log Reduction	Percent Reduction
1-log reduction	90 %
2-log reduction	99 %
3-log reduction	99.9 %
4-log reduction	99.99 %

Log reductions via colony formation method summarized as follows:

1. Fabrics were treated with 200 µL of SOS as per Section 3.2.1.
2. Inoculating bacteria, *Escherichia coli*, was prepared at a concentration of 10^8 CFU/mL as per Section 4.1.1.
3. Treated fabrics were inoculated with 20 µL of bacteria (initial count = $2 \cdot 10^6$ CFU) for 1 hour.
4. Surfaces were diluted with 5 mL of PBS and sonicated for 5 minutes to elute viable bacteria from fabric samples.
5. Solutions were plated onto agar (PCA) at 10 and 100 µL.
6. Plate counts at 10 and 100 µL were averaged and log reductions performed.

Agar tests were repeated in triplicate on cotton fabrics treated with 100 ppm and 1000 ppm Ag. Plate counts were averaged to provide a statistical basis for bacterial log reductions. Results at 10 and 100 µL plating volumes are given in Table 11 and Table 12.

Table 11 Plate counts for 10 µL dispensed on agar, log reduction performed relative to 2(10^6) CFU (EC - excessive counts > 200)

Sample	Control	100 ppm Ag	1000 ppm Ag
A	EC	0	1
B	1	0	0
C	3	0	0
Average	2	0	0.33
Log Reduction	-	NA	0.78

Table 12 Plate counts for 100 µL dispensed on agar, log reduction performed relative to 2(10^6) CFU (EC - excessive counts > 200)

Sample	Control	100 ppm Ag	1000 ppm Ag
A	EC	4	3
B	11	0	0
C	27	2	0
Average	19	2	1
Log Reduction	-	0.97	1.28

The silver organometallic proved extremely effective at reducing bacteria, with zero colony counts observed in the 100 ppm Ag sample plated at 10 µL. As a result, log reductions were unable to be performed. Calculating log reductions for the 100 µL plates show an 89.5 % reduction in bacteria at 100 ppm Ag and a 94.7 % reduction at 1000 ppm Ag, indicating improved antibacterial efficacy correlating with the increase in silver concentration.

Low plate counts observed in experiment indicate that inoculating bacteria concentration may have been too low. Moreover, complete recovery of viable bacteria is not guaranteed due to the porous nature of cotton fibers. Partial recovery may result in reduced plate counts that overestimate the reduction of bacteria. Log reductions applied to silver treated fabrics therefore could only be compared to the control sample. A simplified procedure based on minimum inhibitory concentration that resolves these issues is discussed in Section 4.1.3.

4.1.3 Minimum Inhibition Concentration

As a result of zero plate counts observed in log reduction experiments, the silver-based organometallic was subjected to a more general test that defines the minimum inhibitory concentration (MIC) [42]. For antimicrobial surfaces, the MIC assay determines the minimum concentration of bacteria where complete inhibition of growth occurs. This is accomplished by inoculating treated fabrics at serially diluted concentrations of bacteria before transferring to agar. Viable bacteria favours the nutrient-rich agar environment and naturally begins to migrate. The inoculum concentration where no colony formation is first observed is considered the MIC. Coolmax fabrics were used as substrates due to the

curling effect observed on cotton in disc diffusion tests, Section 4.1.1. Intimate contact with agar is critical to allow proper transfer of CFU to agar.

MIC assay summarized as follows:

1. Sample fabrics were treated with 200 µL of SOS and dried (see Section 3.2.1).
2. Inoculating bacteria, *Escherichia coli*, was prepared at an initial concentration of 10^8 CFU/mL.
3. Serial dilutions of the 10^8 CFU/mL stock were performed to create inoculum at concentrations 10^7 CFU/mL, 10^6 CFU/mL, 10^5 CFU/mL, 10^4 CFU/mL, 10^3 CFU/mL and 10^2 CFU/mL.
4. Treated fabrics were inoculated with 200 µL of each bacteria concentration for 1 hour.
5. Fabric samples were then plated onto agar (PCA) for a contact time of 15 minutes and removed.
6. Agar plates where the incubated at 38 °C for 24 hours to allow for growth of viable bacteria.

Fabric samples were treated at silver concentrations of 100 ppm and 1000 ppm relative to a control sample (0 ppm). Plate counts at each bacterial dilution are listed in Table 13. The inoculum concentration where bacterial growth is completely suppressed is defined as the MIC.

Table 13 Colony formation at various dilutions (EC - Excessive Count > 200 CFU)

Initial Concentration (CFU)	Control (CFU)	100 ppm Ag (CFU)	1000 ppm Ag (CFU)
2E+07	EC	EC	34
2E+06	EC	105	18
2E+05	153	21	5
2E+04	18	5	0
2E+03	7	0	0
2E+02	0	0	0
MIC (% Reduction)	99 %	99.9 %	99.99 %

As a standardized test the MIC protocol was extremely effective in providing accurate analysis of antibacterial efficacy. Bacterial reduction in the control sample was first observed at concentrations of 10^5 CFU, indicating a natural antibacterial property in the base cotton fabric. Complete inhibition of bacteria did not occur until a MIC of 10^2 CFU, a significant reduction of 99 %.

Samples at 100 ppm and 1000 ppm demonstrated high antibacterial ability based on MIC response. A 1-log reduction difference was observed between the two treated samples, correlating well with the proportional logarithmic increase in silver concentration. MIC results confirm the antibacterial properties of the SOSs, promoting complete elimination of up to 99.9 % of bacteria for the primary 100 ppm Ag formulation. The silver-based organometallic was thus determined to be an effective bactericide at the range of concentrations studied. Results from the MIC test is used to validate response in the ATP based approach of Section 4.2.

4.2 Bacterial Adenosine Triphosphate (ATP)

Section 4.2 leverages the biological organic molecule adenosine triphosphate (ATP)—found in all living cells—to measure bacterial activity. ATP is used as store of energy in many biological processes such as nerve signaling, muscle contraction, synthesis of nucleic acids and cellular respiration [43]. ATP is an unstable molecule comprised of an adenine ring, a ribose sugar, and three phosphate groups—structure given in Figure 40. Chemical energy is conserved in the phosphate bonds and is liberated in water by hydrolysis of the third phosphate group to produce adenosine diphosphate (ADP). This reaction releases 7.3 kilocalories per mole of free energy [44]. ADP is recycled and phosphorylated back into ATP via aerobic metabolism. In this manner ATP is analogous to a rechargeable battery.

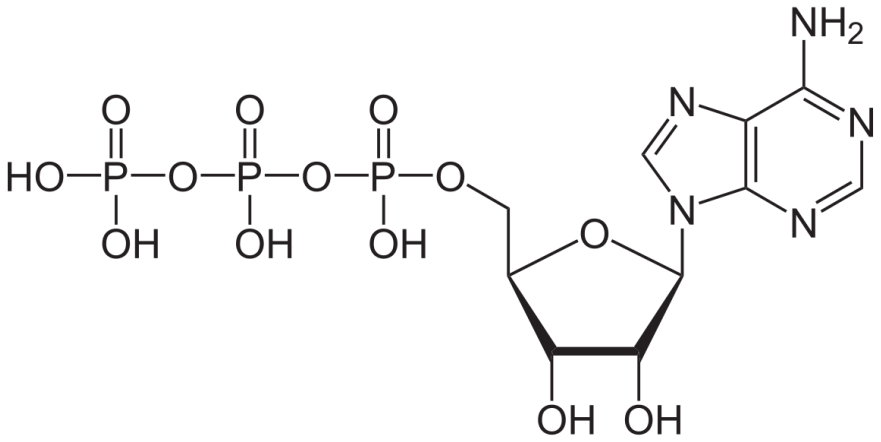

Figure 40 Structure of an ATP molecule [45].

ATP is generated through cellular respiration, an aerobic metabolic process that use biochemical pathways to oxidize organic compounds into ATP and simpler organic compounds. Production of ATP occurs through a series of biochemical reactions—glycolysis, Krebs cycle, and the electron transport chain. As an example, the process is summarized by the complete oxidation of glucose through the following chemical reaction,

$$C_6H_{12}O_6 + 6O_2 \rightarrow 6CO_2 + 6H_2O + energy \tag{4.2}$$

ATP concentration can be measured by the photochemical reaction with the enzyme Luciferase, naturally produced by fireflies. The substrate, luciferin, reacts with ATP to form the intermediate compound luciferyl adenylate. Oxidization of this intermediate compound produces oxyluciferin in an electronically excited state. A return to ground state releases a photon at a specific wavelength measurable by detectors [46]. The concentration of bacterial ATP can thus be correlated to light intensity produced the following reactions,

$$luciferin + ATP \rightarrow luciferyl\ adenylate + PP_i \tag{4.3}$$

$$luciferyl\ adenylate + O_2 \rightarrow oxyluciferin + AMP + energy \tag{4.4}$$

Luminescence is measured using a calibrated photometer, which converts photons into a proportional electrical signal. ATP systems typically use relative light units (RLU) as the unit of measure for ATP, with

the specific ratio of RLU to ATP varying per manufacturer. ATP concentration was measured using an EnSURE system monitor and ATP3000 SuperSnap test swabs manufactured by Hygeina, Camarillo, USA. The ratio of RLU to ATP was evaluated in comprehensive studies performed by food science lab Silliker Group, Chicago, USA—specifications summarized in Table 14.

Table 14 RLU-ATP system specifications for the Hygiena SystemSURE monitor with Hygiena Supersnap swab [47]

RLU/ATP Ratio	Linearity	Output (RLU)		Variation	Sensitivity
(RLU/fmole)	(r)	Blank (0 ATP)	Maximum (1000 fmols ATP)	Coefficient of Variance (%)	Limit of Detection (fmols ATP)
6	0.987	0	4949	9	0.17

ATP concentration in bacteria cultures have been studied by Mempin et al. [48]. Intracellular ATP levels measured in *Escherichia coli* were reported to be between 1–5 mM. Extracellular ATP levels were observed to be regulated by the bacterial growth phase; ATP concentration peaks during the late log phase of growth before decreasing to undetectable levels over 24 hours. Extracellular ATP is thus a dynamic process of ATP release and depletion. Incubation of bacterial cultures for a minimum of 24 hours is therefore necessary to reduce variance in extracellular ATP.

4.2.1 ATP Bacteria Testing on Fabrics

The proposed ATP test is designed as an accelerated method for testing antimicrobial agents on textiles, providing quantitative efficacy without the need for long incubation times. Principles of the test are based on bioluminescent mechanisms of ATP in bacteria. Procedures were based on methods that assess similar cellular metabolic activity—particularly those which have been applied to antimicrobial textiles, such as the MTT and H-thymidine incorporation assays [49]. Concentrations of ATP are measured based on light produced in reaction with the oxidizing agent luciferin. ATP correlates to bacterial activity and can be compared to a control sample to estimate reductions in bacteria. It should be noted that ATP tests are not colony forming tests and do not represent CFU, rather bacterial activity is measured indirectly via a byproduct of cells. The proposed ATP test is therefore not a replacement for microbiological tests but an expediated method to be used in conjunction.

ATP experimental methods summarized as follows:

1. Fabric samples and inoculum were prepared as described in Section **Error! Reference source not found.**.
2. Fabric samples are inoculated with 200 µL of bacteria for 1 hour.
3. Samples are diluted with PBS and sonicated for 5 minutes.
4. 10 µL of recovery solution is pipetted directly onto ATP swabs and RLU measured.

Antibacterial efficacy is determined by percent reduction in RLU values for treated fabrics relative to a control sample,

$$R\ \% = \frac{C_{control} - C_{treated\ sample}}{C_{Control}} \tag{4.5}$$

4.2.2 ATP Test on Treated Textiles

ATP was measured for cotton samples treated at 100 and 1000 ppm Ag, RLU responses plotted in Figure 41. Lower RLU values were observed for higher concentrations of silver, indicating effective reduction in bacteria by the silver-based organometallic. ATP concentration was determined to be extremely sensitive to methods in the recovery stage. Specifically, ATP response was observed to decrease with increasing dilution volumes for all samples. As a result, percent reductions were determined relative to an untreated control at the same dilution. In this manner bacterial activity is compared before and after treatment.

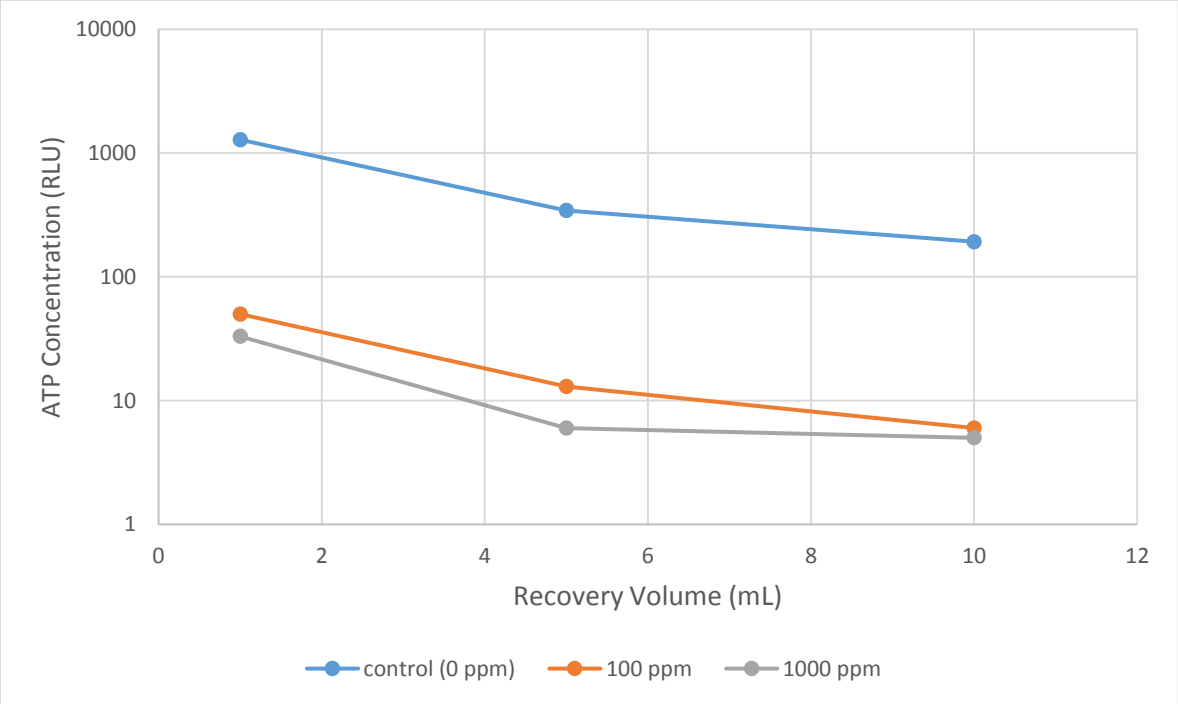

Figure 41 ATP concentration for cotton samples at various dilutions, reference 2(10^7) bacteria count = 7141 RLU.

Relative percent reductions were calculated from RLU values for treated fabrics at three recovery volumes, detailed in

Table *15*. Results show significant reduction in bacteria (> 90 %) for SOSs at both 100 and 1000 ppm. Reductions were averaged across dilutions; low standard deviations in both samples indicate a minimal effect of dilution. A slightly greater reduction was observed in the 1000 ppm Ag treated samples in agreement with standard methods i.e. MIC assay.

Table 15 Percent reduction of bacteria on treated fabrics relative to untreated sample at various dilutions

Ag Concentration		100 ppm Ag	1000 ppm Ag
Recovery Volume (mL)	1	96.1 %	97.4 %
	5	96.2 %	98.3 %
	10	96.9 %	97.4 %
Average		96.4 %	97.7 %
Relative Standard Deviation		0.4 %	0.5 %

4.2.3 ATP Test on Copper Standard

To establish a reference for antibacterial efficacy using ATP, the test was applied to the standard antimicrobial pure copper. Antibacterial efficacy of copper surfaces is well established in EPA protocols, which defines a copper antimicrobial surface as capable of a minimum log-3 reduction of bacteria relative to a steel control [50]. Steel surfaces were thus used as a universal control to compare the treated fabrics to standard copper. Copper and steel square plates (1 inch) were polished to remove any surface oxidation and to allow proper exposure of the metal. The plates were then soaked in ethanol for 10 minutes to eliminate any residual bacteria. Experiments proceed as outlined in the main section. Figure 42 plots ATP concentration for each substrate at various recovery dilutions.

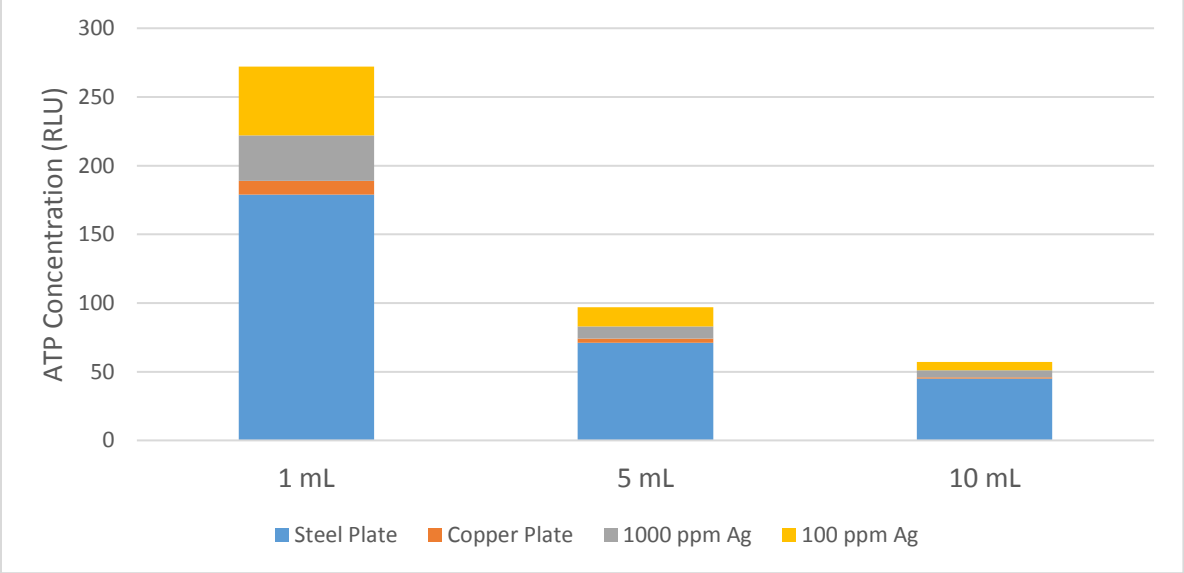

Figure 42 ATP concentration of steel, copper and silver organometallic samples at various dilutions, reference 2(10^7) bacteria count = 7141 RLU.

Percent reductions were performed at each recovery volume relative to the steel control, see Table 16. Averaged results from the copper samples show that a log-3 reduction from steel approximately equates to a 96 % reduction in ATP concentration. Treated fabrics at 100 ppm and 1000 ppm Ag exhibited less ATP reduction compared to copper, with a decrease of 16 % and 10 % respectively.

Large standard deviations observed in the fabric samples are likely due to reductions performed relative to a hard control surface. Fabrics contain porous fibers that can harbor bacteria and limit measurable ATP, acting as a source of variance. In contrast, metal surfaces offer no protection to bacteria which are completely exposed to the antimicrobial element. As a result, it is recommended tested samples be of the same material for improved accuracy.

Table 16 Percent reduction of bacteria on treated fabrics and copper relative to steel control surface at various dilutions

Ag Concentration		100 ppm Ag	1000 ppm Ag	Cu
Recovery Volume (mL)	1	72 %	82 %	94 %
	5	80 %	87 %	96 %
	10	87 %	89 %	98 %
Average		80 %	86 %	96 %
Relative Standard Deviation		7 %	4 %	2 %

Chapter 5 | Conclusions

Analysis via SEM imaging in Chapter 2 confirmed the presence of silver on treated cotton fabrics and revealed the sparse distribution of deposits throughout fibers. Elemental composition of the solid organometallic was determined to be primarily silver by weight—approximately 62 %—with the remaining mass constituting carbon and oxygen elements. Chemical stability of the organometallic in liquid solution was monitored over time revealing a significant drop out of silver when exposed to open environments. Precipitation of silver salts was hypothesized to be a result of high pH in solution. Isolation from external light or the addition of chemical stabilizing agents are recommended to improve the lifetime of the product. Furthermore, silver concentration recovered from cotton fabrics averaged around 51 % of the initially applied amount, with partial loss of silver attributed to the incomplete stripping of silver from fibers.

Quantitative measurement for staining on fabrics was achieved in Chapter 3 using the Nix Pro sensor. Colour difference measured at increasing concentrations of applied silver demonstrated an exponential relation, with imperceptible changes generally below 100 ppm silver. Staining patterns were affected by a combination of the SOS's solvent base and the fiber type. Stains from water-based SOSs on Coolmax fabric would concentrate at edges due to the capillary action of the fibers, resulting in an uneven gradient staining. Direct measurement is not recommended in these cases and averages must be taken. Studies performed at high temperatures—simulating dryer conditions—exacerbated the staining effects observed at standard drying conditions. The Nix Sensor method can be applied to the development of future SOSs to minimize the possibility of staining.

Finally, antibacterial effectiveness of SOSs was studied in Chapter 4. The efficacy of treated fabrics was most accurately determined by minimum inhibitory concentration tests. Results from the MIC test confirm the antibacterial properties of the water-based SOSs, reporting a complete elimination of 99.9 % of bacteria after 15 minutes of contact for the primary 100 ppm silver organometallic formula. Biological studies performed can be used in support of antibacterial claims. In addition, accelerated methods of antibacterial testing proposed by measuring cellular ATP levels correlated well with results determined by the MIC test. Validation tests using standard antibacterial metals showed comparable killing power between the SOSs and standard copper metal. ATP values measured in this study can be used as reference to estimate antibacterial efficacy in future SOSs or any general antibacterial surface.

References

[1] J. Clement and P. Jarrett, "Antibacterial Silver," *Metal-Based Drugs,* vol. 1, no. 5, pp. 467-482, 1994.

[2] The Editors of Encyclopaedia Britannica, "Antimicrobial agent," 5 February 2016. [Online]. Available: https://www.britannica.com/science/antimicrobial-agent. [Accessed 6 November 2019].

[3] B. Deerin, "Antimicrobial Fibers History, Uses, Applications," Textile World, 21 February 2017. [Online]. Available: https://www.textileworld.com/textile-world/features/2017/02/antimicrobial-fibers-history-uses-applications/. [Accessed 28 September 2019].

[4] D. Morais, R. Guedes and L. Maria, "Antimicrobial Approaches for Textiles: From Research to Market," *Materials,* vol. 9, no. 498, 2016.

[5] L. Windler, M. Height and B. Nowack, "Comparative evaluation of antimicrobials for textile applications," *Environmental International,* vol. 53, pp. 62-73, 2013.

[6] B. Bassler, "Bacterial Communication: Quorum Sensing in Bacteria," [Online]. Available: http://faculty.ccbcmd.edu/courses/bio141/lecguide/unit1/shape/quorum_sensing.html. [Accessed 2 October 2019].

[7] M. Gangan and C. Athale, "Threshold effect of growth rate on population variability of Escherichia coli cell lengths," *Royal Society Open Science,* vol. 4, no. 2, 2017.

[8] S. Henkel and J. Setchell, "Group and kin recognition via olfactory cues in chimpanzees (Pan troglodytes)," *Proceedings of the Royal Society B ,* vol. 285, no. 1889, 2018.

[9] M. Troccaz, N. Gaïa, S. Beccucci, J. Schrenzel, I. Cayeux, C. Starkenmann and V. Lazarevic, "Mapping axillary microbiota responsible for body odours using a culture-independent approach," *Microbiome,* vol. 3, no. 3, 2015.

[10] R. Mcqueen, M. Keelan and S. Kannayiram, "Determination of Antimicrobial Efficacy for Textile Products Against Odor-Causing Bacteria," *American Association of Textile Chemists and Colorists Review,* vol. 4, no. 10, pp. 58-63, 2010.

[11] T. H. Lam, D. Verzotto, P. Brahma, A. Ng, P. Hu, D. Schnell, J. Tiesman, R. Kong, T. Ton, J. Li, M. Ong, Y. Lu, D. Swaile, P. Liu, J. Liu and N. Nagarajan, "Understanding the microbial basis of body odor in pre-pubescent children and teenagers," *Microbiome,* vol. 6, no. 213, 2018.

[12] S. Modak and C. J. Fox, "Binding of silver sulfadiazine to the cellular components of Pseudomonas aeruginosa," *Biochem Pharmacology,* vol. 1, no. 22, p. 19, 1973.

[13] I. Harrison and F. Spada, "Hydrogels for Atopic Dermatitis and Wound Management: A Superior Drug Delivery Vehicle," *Pharmaceutics,* vol. 10, no. 2, p. 71, 2018.

[14] Q. Shia, N. Vitchulia, J. Nowakb, J. Caldwell, F. Breidt, M. Bourham, X. Zhang and M. McCordae, "Durable antibacterial Ag/polyacrylonitrile (Ag/PAN) hybrid nanofibers prepared by atmospheric plasma treatment and electrospinning," *European Polymer Journal,* vol. 47, no. 7, pp. 1402-1409, 2011.

[15] M. Patra and N. Metzler-Nolte, "Small organometallic compounds as antibacterial agents," *Dalton Transactions,* no. 41, 2012.

[16] E. Campbell, R. He and M. Mayer, "Conductive pathway on cotton fabric created using solution with silver organometallic compound," *Materials Research Express,* vol. 4, 2017.

[17] A. Abou-okeil, "Ag Nanoparticles Growing onto Cotton Fabric Using Chitosan as a Template," *Journal of Natural Fibers,* vol. 9, no. 2, pp. 61-72, 2012.

[18] D. Puchowicza, P. Giesza, M. Kozaneckib and M. Cieślaka, "Surface-enhanced Raman spectroscopy (SERS) in cotton fabrics analysis," *talanta,* no. 195, pp. 516-524, 2019.

[19] M. Üreyen and C. Aslan, "Determination of silver release from antibacterial finished cotton and polyester fabrics into water," *The Journal of The Textile Institute,* vol. 7, no. 108, pp. 1128-1135, 2017.

[20] H. Liu, M. Lv, B. Deng, J. Li, M. Yu, Q. Huang and C. Fan, "Laundering durable antibacterial cotton fabrics grafted with pomegranate-shaped polymer wrapped in silver nanoparticle aggregations," *Scientific Reports,* vol. 4, 2014.

[21] H. Won, H. Nersisyan, C. Won, J.-M. Lee and J.-S. Hwang, "Preparation of porous silver particles using ammonium formate and its formation mechanism," *Chemical Engineering Journal,* no. 156, pp. 459-464, 2010.

[22] G. El-Nagar, R. Sarhan, A. Abouserie, N. Maticiuc, M. Bargheer, I. Lauermann and C. Roth, "Efficient 3D-Silver Flower-like Microstructures for Non-Enzymatic Hydrogen Peroxide Amperometric Detection," *Scientific Reports,* no. 7, 2017.

[23] D.-Y. Shin and I. Kim, "Self-patterning of fine metal electrodes by means of the formation of isolated silver nanoclusters embedded in polyaniline," *Nanotechnology,* no. 20, 2009.

[24] R. Mohadi, R. Purba, D. Rohendi and A. Lesbani, "Kinetics and Thermodynamics Interaction Between Bentonite Inserted Organometallic Compounds [Cr 3 O(OOCH) 6 (H 2 O) 3](NO 3) With Methylene Blue Dye In Aqueous Medium.," in *IOP Conference Series: Materials Science and Engineering*, 2018.

[25] K. Kavkler and A. Demšar, "Examination of cellulose textile fibres in historical objects by micro-Raman spectroscopy," *Spectrochimica Acta Part A Molecular and Biomolecular Spectroscopy,* vol. 2, no. 78, pp. 740-746, 2011.

[26] Porex Filtration, "Heavy Metal Removal From Wastewater by Precipitation and Microfiltration," [Online]. Available: http://www.porexfiltration.com/learning-center/technology/precipitation-microfiltration/. [Accessed 18 October 2019].

[27] "Earth's Lab," 8 August 2018. [Online]. Available: https://www.earthslab.com/physiology/structure-eye-functions-accessory-structures/.

[28] S. Nakata, E. Phillips and V. Goidts, "Emerging role for leucine-rich repeat-containing G-protein-coupled receptors LGR5 and LGR4 in cancer stem cells," *Cancer management and research,* no. 6, pp. 171-180, 2014.

[29] A. Terakita, "The opsins," *Genome Biology,* vol. 6, no. 3, p. 213, 2005.

[30] "University of New Mexico," [Online]. Available: https://www.unm.edu/~toolson/human_cone_response.htm. [Accessed 20 September 2019].

[31] C. Abraham, "A Beginner's Guide to (CIE) Colorimetry," 10 September 2016. [Online]. Available: https://medium.com/hipster-color-science/a-beginners-guide-to-colorimetry-401f1830b65a. [Accessed 20 September 2019].

[32] R. Feynman, "Color Vision," in *The Feynman Lectures on Physics, Volume I*, Addison-Wesley, 1963.

[33] G. Wyszecki and W. Stiles, Color Science: Concepts and Methods, Quantitative Data and Formulae, Wiley-Interscience, 1967.

[34] K. Houser, "Spectral power distribution of D65," Nebraska, 2006.

[35] Z. Schuessler, "Delta E 101," 2016. [Online]. Available: http://zschuessler.github.io/DeltaE/learn/#toc-delta-e-101. [Accessed 21 September 2019].

[36] Nix Sensor Ltd., "Nix Pro Specification," [Online]. Available: https://www.nixsensor.com/nix-pro/. [Accessed 6 November 2019].

[37] O. M. Laboratory, "United States Environmental Protection Agency," 2017. [Online]. Available: https://www.epa.gov/pesticide-analytical-methods/antimicrobial-testing-methods-procedures-developed-epas-microbiology. [Accessed 28 September 2019].

[38] J. Hudzicki, "Kirby-Bauer Disk Diffusion Susceptibility Test Protocol," American Society for Microbiology, 2009.

[39] M. Hardwick, T. Walsh and M. Cotton, "Fabric Challenge Assays: New Standards for the Evaluation of the Performance of Textiles Treated with Antimicrobial Agents," *Pesticide Formulation and Delivery Systems,* vol. 32, pp. 125-138, 2013.

[40] AATCC, "TM-100 Test Method for Antibacterial Finishes on Textile Materials: Assess," American Association of Textile Chemists and Colorists, RTP, 2004.

[41] ASTM, "Standard Test Method for Determining the Antimicrobial Activity of Antimicrobial Agents Under Dynamic Contact Conditions," ASTM International, West Conshohocken, 2013.

[42] "Determination of minimum inhibitory concentrations," *The Journal of Antimicrobial Chemotherapy,* vol. 1, no. 48, pp. 5-16, 2001.

[43] P. Jurtshuk, "Bacterial Metabolism," in *Medical Microbiology*, Galveston, The University of Texas Medical Branch at Galveston, 1996.

[44] R. Nave, "Adenosine Triphosphate," Hyperphysics, [Online]. Available: http://hyperphysics.phy-astr.gsu.edu/hbase/Biology/atp.html. [Accessed 28 September 2019].

[45] "Adenosine triphosphate," Wikipedia, [Online]. Available: https://en.wikipedia.org/wiki/Adenosine_triphosphate. [Accessed 28 September 2019].

[46] W. McElroy and A. Green, "Function of adenosine triphosphate in the activation of luciferin," *Archives of Biochemistry and Biophysics,* vol. 64, no. 2, pp. 257-271, 1956.

[47] Silliker, Inc., "Performance Evaluation of Various ATP Detecting Units," Silliker, Inc, Chicago, 2009.

[48] R. Mempin, H. Tran, C. Chen, H. Gong, K. Ho and S. Lu, "Release of extracellular ATP by bacteria during growth," *BMC Microbology,* vol. 13, no. 301, 2013.

[49] H. Haase, L. Jordan, L. Keitel, C. Keil and B. Mahltig, "Comparison of methods for determining the effectiveness of antibacterial functionalized textiles," *PLoS ONE,* vol. 11, no. 12, 2017.

[50] Environmental Protection Agency, "Protocol for the Evaluation of Bactericidal Activity of Hard, Non-porous Copper Containing Surface Products," 2016.

[51] A. Reichenbach and A. Bringmann, Retina (5th Edition), Saunders, 2013.

[52] G. Tortora, B. Funke and C. Case, Microbiology : An Introduction, Pearson Education, 2010.

[53] J. Clement and P. Jarrett, "Antibacterial Silver," *Metal Based Drugs,* vol. 1, no. 5, pp. 467-482, 1994.

[54] J. Wright, K. Lam and R. Burrell, "Wound management in an era of increasing bacterial antibiotic resistance: a role for topical silver treatment," *American Journal of Infection Control,* vol. 26, no. 6, pp. 572-577, 1998.

[55] X. Cai and A. Zhai, "Preparation of microsized silver crystals with different morphologies by a wet-chemical method," *Rare Metals,* vol. 29, no. 4, pp. 407-412, 2010.

[56] M. Yazdanshenas and M. Shateri-Khalilabad, "In situ synthesis of silver nanoparticles on alkali-treated cotton fabrics," *Journal of Industrial Textiles,* vol. 4, no. 42, pp. 459-474, 2013.